Climate Data Record (CDR) Program

Climate Algorithm Theoretical Basis Document (C-ATBD)

SSMI(S) Brightness Temperature - RSS

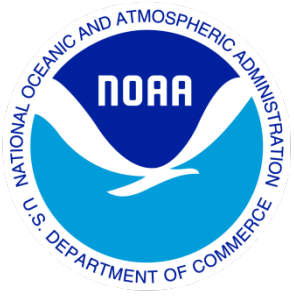

CDR Program Document Number: CDRP-ATBD-0100
Configuration Item Number: 01B-05
Revision 3 / March 30, 2018

REVISION HISTORY

Rev.	Author	DSR No.	Description	Date
1	Carl Mears, RSS	DSR-105	Initial Submission to CDR Program	06/14/2011
2	Carl Mears, RSS	DSR-388	Revised Submission-Section 3 entirely rewritten. Minor edits were performed to reflect the version number change elsewhere in the document.	3/28/2013
3	Carl Mears, RSS	DSR-1256	Revised Submission to CDR Program due to upgrade to v8 for F18.	03/30/2018

TABLE of CONTENTS

Update this table by right click (Windows) or Control-click (Mac OS-X) and selecting the "Update Field" option from the context menu.

LIST of FIGURES

Search Word online help for "Add or delete captions" for assistance with this table.

LIST of TABLES

Search Word online help for "Add or delete captions" for assistance with this table.

1. Introduction

1.1 Purpose

The purpose of this document is to describe the algorithm used to create the RSS Version-7 SSM/I Fundamental Climate Data Record (FCDR) and Version-8 SSMIIS Fundamental Climate Data Record (FCDR), using the DMSP SSM/I and SSMIS series of instruments. The actual algorithm is defined by the computer program (code), and thus the intent here is to provide a guide to understanding that algorithm, from both a scientific perspective and in order to assist a software engineer performing an evaluation of the code.

1.2 Definitions

Following is a summary of the symbols used to define the algorithm.

Γ = Antenna Function

Ψ = Simplified RTM

T_s = Sea Surface Temperature

W = Surface Wind Speed

ϕ_w = Wind Direction

V = Total Column Water Vapor

L = Total Column Liquid Water

T_A = Antenna Temperature

T_B = Brightness Temperature

η = spillover

χ = cross-polarization coupling

β = sun zenith angle

α = sun azimuth angle

λ = non-linearity adjustment amplitude

θ_i = earth incidence angle

ϕ_r = relative angle between the wind direction and the SSM/I azimuth look direction

$\psi(\omega)$ = scan angle correction factor

ξ = target factor

φ = position of the satellite in its orbit

1.3 Referencing this Document

This document should be referenced as follows:

SSMI(S) Brightness Temperature – RSS - Climate Algorithm Theoretical Basis Document, NOAA Climate Data Record Program CDRP-ATBD-0100 Rev. 3 (2018). Available at http://www.ncdc.noaa.gov/cdr/operationalcdrs.html

1.4 Document Maintenance

This document is under version control in the CDR Program Library. The information in this document applies to the v8.0 of the archived data. Further versions of the product will be accompanied by an update to this C-ATBD and other documentation, as needed.

2. Observing Systems Overview

2.1 Products Generated

The Special Sensor Microwave Imagers (SSM/I) are a series of six satellite radiometers that have been in operation since 1987 under the Defense Meteorological Satellite Program (DMSP). These satellite sensors measure the natural microwave emission coming from the Earth's surface in the spectral band from 19 to 85 GHz. These emission measurements contain valuable information on many important climate variables including winds over the ocean, moisture and rain in the atmosphere, sea ice, and snow cover. However, the extraction of this information from the raw satellite measurements is a complicated process requiring considerable care and diligence. The first step in the process is the generation of Fundamental Climate Data Records (FCDR) of the sensor measurements in term of antenna temperatures (T_A) and brightness temperatures (T_B). It is absolutely essential that proper satellite inter-calibration methods be employed when producing these SSM/I FCDRs.

2.2 Instrument Characteristics

The radiometric characteristics of the seven SSMIS channels are listed in Table 1. These channels were selected to achieve specific objectives for measuring parameters. For example, a channel with a center frequency of 22.235 GHz was included in order to obtain estimates of atmospheric water vapor. The 19 and 37 GHz channels were used to achieve the maximum transfer of scientific experience and algorithms from the ESMR and SMMR instruments. The 85.5 GHz channels were chosen in order to more effectively measure rain and cloud properties. The channel bandwidths were chosen as a compromise between spectral sensitivity (requiring the narrowest spectral intervals) and sensor noise. For broadband signals, the measurement uncertainty due to noise is inversely proportional to the square root of the bandwidth, so larger bandwidths generally result in more accurate measurements.

CHANNEL ABBREVIATION	CENTER FREQUENCY (GHz)	CENTER WAVELENGTH (cm)	BANDWIDTH (MHz)	POLARIZATION	INTEGRATION TIME (ms)
19V	19.35	1.549	355	Vertical	7.95
19H	19.35	1.549	357	Horizontal	7.95
22V	22.235	1.348	401	Vertical	7.95
37V	37.0	0.810	1616	Vertical	7.95
37H	37.0	0.810	1545	Horizontal	7.95
91V	91.66	0.327	1418	Vertical	3.89
91H	91.66	0.327	1411	Horizontal	3.89

Table 1: SSMIS Channel characteristics (Aerojet).

3. Algorithm Description

3.1 Algorithm Overview

The RSS SSM/I and SSMIS FCDR datasets have incorporated geolocation corrections, sensor calibration (including cross-scan biases), and quality control procedures in a consistent way for the entire 20-year SSM/I and SSMIS dataset. This document describes the methods used to calibrate the F18 SSMIS instrument using RSS Version 8 methods. In version 8, all satellites will be intercalibrated using TMI and GMI collocations, except for SSM/I F08 amd F10, which do not overlap with either of these satellites. The recalibration is an on-going effort. We anticipate that all SSM/I and SSMIS instruments will be recalibrated using V8 methods in the near future.

3.2 Processing Outline

The processing outline for the RSS SSM/I FCDR is summarized in Figure 1, which includes the basic elements such as input, output, and intercalibration as well as the conversion of the data to netCDF-4.

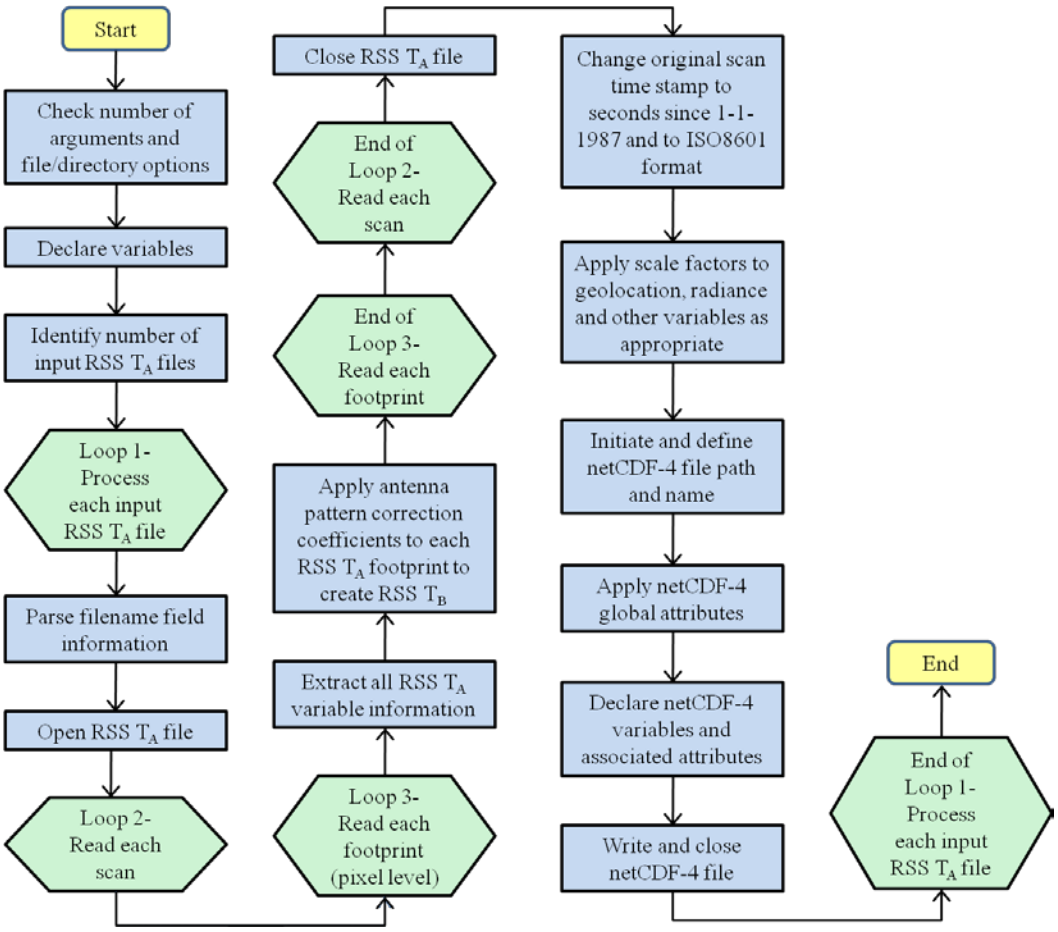

Figure 1: Flow chart for the creation of RSS Version-6 SSM/I FCDR

3.3 Algorithm Input

3.3.1 Primary Sensor Data

Original SSM/I and SSMIS antenna temperature data is generated after four processes: raw data acquisition, raw data unpacking, Earth location and tagging, and on-board calibration. Data is stored at RSS in a flat binary format, with one file for each SSM/I or SSMIS orbit. These files are the input data for the TA to TB algorithm described below.

3.3.2 Ancillary Data

The algorithm uses several sources of ancillary data. These are described below.

bad_orbits_f18.txt This is a text file containing a list of orbits with corrupted data that should be excluded from further processing.

3.3.3 Derived Data

Not applicable

3.3.4 Forward Models

Not applicable

3.4 Theoretical Description

Overview of Calibration Procedure

The first step in the calibration is to determine the antenna spillover η and cross polarization coupling χ, thereby establishing the absolute calibration of the SSM/I brightness temperatures. A prerequisite is to require that the $\mathbf{E_p}$ retrievals agree with *in situ* observation in an unbiased sense. The absolute calibration of wind speed is determined from anemometers on moored buoys that are part of the NDBC, TAO, TRITON, and PIRATA arrays. Water vapor absolute calibration is based on radiosonde and GPS measurements. For liquid cloud water, there are no *in situ* measurements extensive and accurate enough to meet our requirements. In this case, we use a statistical histogram method based on the fact that a significant portion of the SSM/I measurements will be free of clouds. This fact established a well determined zero-point for a histogram of cloud water. See *Wentz* [1997] for details. The absolute calibration criterion then requires that the mission-averaged T_A equals the RTM T_A

$$\langle \mathbf{T_A} \rangle = \langle \mathbf{T_{A,rtm}} \rangle \equiv \left\langle \Gamma\left[\Psi\left(\mathbf{E_p} \right) \right] \right\rangle \tag{11}$$

where the brackets denote an average over the entire mission of a specified SSM/I or SSMIS. The antenna parameters η and χ, which are the implicit arguments of Γ, are then adjusted to satisfy the equality, as is described in Section 3.4.4. Early on in the calibration process, $\mathbf{E_p}$ comes from earlier versions of SSM/I or SSMIS processing and from other collocated satellites like WindSat. As the calibration process converges, $\mathbf{E_p}$ is the retrievals from the particular SSM/I or SSMIS being calibrated. Hence, a second instrument is not required by (11). The only requirement is that $\mathbf{E_p}$ is unbiased relative to the *in situ* observations. A final, small adjustment to η and χ is done at the end of the calibration procedure to ensure precise inter-satellite agreement of the geophysical retrievals, as is discussed later in this section.

The second step in the calibration is to find the relative calibration errors $\mathbf{\Delta T_A}$ for the 7 channels. These errors are subtracted from $\mathbf{T_{A0}}$, which is the T_A measurement derived from the radiometer counts given by (19) in Section 3.4.3, in order to obtained the 'true' antenna temperature $\mathbf{T_A}$:

$$\mathbf{T_A} = \mathbf{T_{A0}} - \mathbf{\Delta T_A} \tag{12}$$

The relative errors depends on a number of parameters such as scan position, solar angles, position in orbit, etc., and these are listed later in this section. A given relative error is derived so that its mission average is near zero:

$$\langle \Delta \mathbf{T_A} \rangle \approx 0 \qquad (13)$$

In practice, the mission-average relative error will have a small bias depending on the details of how the mission-average is done, but in general the bias is less than 0.1 K, which is much smaller than the biasing due to the adjustments made to the antenna spillover and coupling. So the η, χ adjustment drives the absolute calibration.

Two types of T_A inter-comparisons are done as represented by the following equations.

$$\delta \mathbf{T_A}(i,j) = \mathbf{T_A}(i) - \mathbf{T_{A,rtm}}(j) \qquad (14)$$

$$\delta \mathbf{T'_A}(i,j) = \mathbf{T'_A}(i) - \mathbf{T'_A}(j) \qquad (15)$$

where we have introduced the indices *i* and *j* as arguments to denote a pair of collocated radiometer measurements. The first type of comparison (14) is between the T_A measurement of one radiometer versus the RTM T_A predicted using the E_p retrievals from a second instrument. The second type of comparison (15) is the same as the first, except that the T_A measurements are first normalized to a common incidence angle and common η and χ. In addition, the normalization also removes the effect of wind direction. This normalization, which is denoted by the prime symbol, is accomplished by equations (9) and (10) and is intended to make the T_A measurements from two imaging radiometers directly comparable. For the first type of inter-comparison, the collocation criterion is based on daily, ¼° latitude/longitude maps. Separate maps are made for the ascending and descending orbit segments. The collocation criterion is that for a given map, a ¼° cell must contain observations from both instruments. The collocation criterion is the same for the second type of inter-comparison except the maps are 5-day (pentad), 1° latitude/longitude maps. For V8 processing, all calibration is based on comparison with either the GPM microwave imager (GMI) or the TRMM microwave imager (TMI). Because these two instruments are in rapidly precessing orbits, they are closely collocated in time with any polar orbiter fairly often, and a collocation dataset with the time distance clustered around zero difference can be constructed, minimizing problems due to any diurnal cycle present.

We consider the most important scientific criterion for inter-satellite calibration is that the collocated geophysical retrievals from pairs of SSM/Is precisely agree. This is particularly important when constructing multi-decadal time series from the 25 years of SSM/I observations. Thus as the final step in the calibration procedure, we require the wind, vapor, and cloud retrievals from the pairs of SSM/I to precisely agree. In this case, the inter-satellite comparison is represented by

$$\delta \mathbf{E_p}(i,j) = \mathbf{E_p}(i) - \mathbf{E_p}(j) \qquad (16)$$

The $\delta \mathbf{E_p}(i,j)$ differences for the 7 primary overlaps are minimized by making small adjustments to the antenna parameters η and χ. Adjustments to η and χ produce changes in the retrievals as indicated by (6). While minimizing $\delta \mathbf{E_p}(i,j)$, we continue to required that (11) is satisfied as closely as possible. Imposing these two constraints simultaneously (i.e.,

the minimization of $\mathbf{\delta E_p}(i,j)$ and the T_A agreement with the RTM) provides the final values for η and χ. When averaged over the overlap periods, the procedure minimizes the inter-satellite wind and vapor differences to about 0.01 m/s and 0.01 mm. After accounting for diurnal variation, inter-satellite cloud differences are minimized to 0.0002 mm. In addition, the mission averaged T_A minus $T_{A,rtm}$ differences are typically 0.05 K.

There are 5 kinds of relative T_A adjustments:

$$\mathbf{\Delta T_A = \Delta T_{A,\omega} + \Delta T_{A,ht} + \Delta T_{A,isat} + \Delta T_{A,drift} + \Delta T_{A,tf} \equiv \sum_{k=1}^{5} \Delta T_{A,k}} \qquad (17)$$

where:

$\mathbf{\Delta T_{A,\omega}}$ is the along-scan adjustment (Section 3.4.5)

$\mathbf{\Delta T_{A,ht}}$ is the adjustment to the hot target temperature (Section 3.4.6)

$\mathbf{\Delta T_{A,isat}}$ is an adjustment that is unique and specific for the F08, F10, and F15 SSM/I (Sections 3.4.7, 3.4.8, and 3.4.9)

$\mathbf{\Delta T_{A,drift}}$ is a small drift correction applied to F11 and F13 SSM/I (Section 3.4.10)

$\mathbf{\Delta T_{A,tf}}$ is the 'target factor' adjustment (Section 3.4.11)

These adjustments are found so as to minimize either $\mathbf{\delta T_A}(i,j)$ or $\mathbf{\delta T'_A}(i,j)$ as is explained in the subsequent sections.

The adjustments are derived one at a time. Once a given adjustment is found, it is applied to the T_A measurement, and then the next adjustment is found. Once all adjustments are found, we repeat the procedure and find residual adjustments. The residual adjustments are very small (i.e., we get nearly the same adjustment the second time around). For example according to this procedure, when equation (14) to find the n^{th} adjustment $\mathbf{\Delta T_{A,n}}$, the value of $\mathbf{T_A}$ in (14) is

$$\mathbf{T_A = T_{A0} - \sum_{k \neq n} \Delta T_{A,k}} \qquad (18)$$

which says that all adjustments other than the adjustment currently being derived are applied to $\mathbf{T_{A0}}$. The same holds true when equation (15) is being used to derive the adjustment.

Using inter-satellite comparisons to find the $\mathbf{\Delta T_A}$ risks the possibility of calibration errors from one sensor aliasing into another. We call this sensor error crosstalk. To assess this problem, we experimented with many variations of the calibration procedure presented here, such as using different pairs of SSM/Is to derive the same adjustments. For most types of errors, sensor error crosstalk does not appear to be a problem. As an example, when finding the along-scan adjustment $\mathbf{\Delta T_{A,\omega}}$, a given along-scan cell position for the first

SSM/I will tend to randomly collocate with all the cell positions for the second SSM/I. As a result, the ω-errors in the first SSM/I do not alias into $\mathbf{\Delta T_{A,\omega}}$ for the second SSM/I. Furthermore, on the second iteration of the calibration procedure, the errors in the reference SSM/I are mostly removed. The one case where sensor error crosstalk is of concern is the F13 time drift, which is discussed in Section 3.4.10.

Another question on the robustness of the calibration procedure is the orthogonality of the 5 adjustments. Can a given calibration error be represented by more than one type of adjustment? The 5 types of adjustments have been designed to be dissimilar so as avoid this problem. Also, we have gone through many iterations of the calibration process, and the order of finding the 5 adjustments did not seem to really matter as long as two complete iterations of all 5 adjustments is done. Furthermore, any creeping of a calibration error from one type of adjustment to another has little effect on the overall calibration because the adjustments are added together. The only possible problem is the interpretation of the individual errors sources may be a bit skewed.

A useful calibration tool is the degree of closure as expressed by (8), or equivalently by (14) with $i = j$. It would be very convenient if $\mathbf{\delta T_{A,closure}}$ could be used to infer the T_A adjustments because one would then not need to rely on collocations with another SSM/I. However, if the $\mathbf{E_P}$ from the same satellite to compute $\mathbf{T_{A,rtm}}$, then the errors in $\mathbf{E_p}$ due to calibration errors $\mathbf{\Delta T_A}$ would be highly correlated with $\mathbf{\Delta T_A}$, and this correlation would tend to hide and/or distort the derivation of $\mathbf{\Delta T_A}$. This is why we use the $\mathbf{E_P}$ from a different SSM/I to compute $\mathbf{T_{A,rtm}}$. The E_p errors from a second SSM/I are much less correlated with the $\mathbf{\Delta T_A}$ errors of the first SSM/I. That is not to say $\mathbf{\delta T_{A,closure}}$ is not useful. In fact, it is an extremely useful tool for verification and diagnosing residual calibration error as is shown in Section 3.4.7 for the F08 SSM/I. The diagnostic $\mathbf{\delta T_{A,closure}}$ is best used as a final step after all known calibration errors are removed.

Unadjusted Antenna Temperature

In computing the unadjusted SSM/I antenna temperature, the basic assumption is that the radiometer output voltage expressed as counts is linearly related to the input power at the feedhorn expressed as T_A, with a small quadratic adjustment. Under these assumptions, the unadjusted antenna temperature is

$$T_{A0} = \frac{(T_h - T_c)C_e + T_c C_h - T_h C_c}{C_h - C_c} \qquad (19)$$

where the subscript *0* denotes no adjustments have been made. The terms C_c, C_h, and C_e are the radiometer counts when the radiometer is looking at the cold calibration target, the hot calibration target, and the earth scene, respectively. The temperatures T_c and T_h are the effective temperatures of the cold and hot calibration targets. Equation (19) is simply expressing the assumption that the radiometer counts vary linearly as the scene temperature varies from T_c to T_h.

The first difficulty in the calibration process is accurately specifying T_c and T_h. For example, the cold target is a mirror pointing towards cold space, which has a temperature of 2.73 K (i.e., the cosmic background temperature). However, if the mirror is not a perfect reflector or if the mirror is receiving some radiation from other sources such as the spacecraft or the Earth, the true value for T_c will be greater than 2.73 K. The specification of T_h is even more difficult. In this case, one must infer T_h from thermistor readings attached to the hot target. There will be some error in using these readings to estimate the effective emission temperature of the hot target. For example, thermal gradients, both horizontal and vertical, over the extent of the hot target will cause problems. SSM/I has only 3 thermistors attached to the hot target.

Our specification of the cold target temperature is

$$T_c = T_{c,plk} + \delta T_c \tag{20}$$

The first term $T_{c,plk}$ is the Planck-adjusted value of cold space. The relationship between radiation intensity and temperature is given by Planck's law. In the lower microwave spectrum, this relationship is nearly linear and the Rayleigh-Jeans approximation is used. However as the frequency increases, the Rayleigh-Jeans approximation begins to break down. This effect can be compensated for by adjusting the cold space temperature. By doing this, one can continue to assume a linear relationship between radiation and temperature. This is standard practice and the value for $T_{c,plk}$ is 2.752, 2.761, 2.822, and 3.203 K for the four SSM/I frequencies (19, 22, 37, and 85 GHz). The second term δT_c is a small offset we apply to account for radiation coming from sources other than cold space such as the spacecraft and Earth. A value of δT_c = 0.3 K is used for all channels and all SSM/Is. This value assumes 0.2% of the radiation comes from the spacecraft and earth, which have a typical temperature of 150 K. We know the effective temperature of the cold target must be higher than cold space, and the inclusion of δT_c is a small hedge for this. We use this 0.3 K offset for all satellite MW imagers including AMSR-E, WindSat, TMI, and SSM/IS.

Our specification of the hot target temperature is

$$T_h = T_{h,therm} + \delta T_h \tag{21}$$

The first term $T_{h,therm}$ is the hot target temperature derived just from the thermistors measurements, and the second term δT_h is a small offset we apply to account for an overall bias in the effective hot target temperature. A value of δT_h = −1.0 K is used for all channels and all SSM/Is. The inclusion of δT_h results in slightly better agreement between the antenna spillover values derived herein and pre-launch values, as is discussed in Section 5. $T_{h,therm}$ is given by

$$T_{h,therm} = t_h + \xi\left(t_p - t_h\right) \tag{22}$$

The temperature t_h is the average of the 3 thermistor readings attached to the hot target and the temperature t_p is the reading from the single thermistor on the SSM/I drum plate facing the hot target. The coefficient ξ is a value derived from prelaunch thermal-vacuum measurements, and its value is 0.01 [*Hollinger et al.*, 1987]. Equation (22) is saying 99% of the hot target radiation is coming from the hot target itself and 1% of the radiation is coming from the reflection of the drum face off the hot target. For the F13 SSM/I, only hot-target thermistor 2 is used for t_h because the other 2 thermistors displayed considerable noise [*Colton and Poe*, 1999].

Noise in C_c and C_h is reduced by averaging measurements from adjacent scans. We use a time window of ±12 seconds centered on the scan being processed. If there are no data gaps, this time window will include 13 scans. For the 19-37 GHz channels, calibration counts are only collected every other scan. For 85 GHz, calibration counts are collected every scan. For each scan, 5 calibration measurements are taken of the cold target and another 5 for the hot target. Thus our ±12 seconds time window provides 35 cold counts and 35 hot counts for each of the lower-frequency channels and 65 counts at 85 GHz. This is a sufficient number of samples to reduce the noise in the calibration counts to an acceptable level.

In a second step, a small non-linearity correction is applied to T_A.

$$T_A = T_{A0} - 4\lambda X\left(1 - X\right), X = \frac{\left(T_A - T_c\right)}{T_h - T_c}$$

Here, λ is the maximum difference from the linear result, which occurs for T_{A0} values halfway between T_h and T_c. The values for X for each of the 7 channels for F18 are shown in the Table 2

Table 2. Values of the non-linearity adjustment parameter λ for F18.

19V	19H	23V	37V	37H	92V	92V
0.720	0.720	0.793	0.773	0.773	0.976	0.976

In previous versions (Version 6 and Version 7), non-linearity was addressed via the so-called target factor adjustments. With the more direct nonlinearity adjustments described above, these adjustments are no longer needed. These are made possible by using GMI as a calibration reference. Version 6 and 7 calibration began with the first SSM/I (F08) and carried the calibration forward to more recent satellites. Version 8 takes the opposite approach. The calibration originates with the recent GPM Microwave Imager (GMI) instrument on the Global Precipitation Mission (GPM) satellite, and then proceeds backwards to earlier instruments, including SSMIS F18. The reason for this change is that the calibration of the GMI instrument is better understood than any previous instrument. This is in part because in addition to cold space and warm target calibration points, GMI

includes an on-board noise source that injects ~100K of noise into the radiometer system, allowing for 2 additional calibration points, cold space + 100K, and the warm target + 100K. These additional points allow the non-linearity of the radiometer to be precisely measured for the first time. This, in turn, allows us to more precisely tie the absolute calibration of the GMI instrument to our radiative transfer model over a wide range of scene brightness temperatures, including both ocean (intermediate TB) and land (high TB). The GMI calibration procedure is described in detail in Wentz and Draper [2016].

The precise calibration of the GMI instrument allows us to develop a detailed model of the seasonal and diurnal variation of the brightness temperature of the surface emission from high TA land sources, in particular from the Amazon rain forest, which we have found to be relatively stable from year to year. This in turn allows the use of the Amazon as a third calibration point to assess the absolute calibration and non-linearity of other satellites, including F18. Note that without the third point, it is impossible to determine whether observed intersatellite differences are due to absolute calibration offsets, or to differences in radiometer non-linearity. In version 8, the non-linearity is determined as part of the calibration procedure by comparing collocated observations from different satellites over both ocean target and the Amazon rain forest.

In Figure 2, we show that several V8 calibrated satellites agree over the Amazon rainforest to ~0.1K. Similar agreement is achieved with the same calibration over ocean targets.

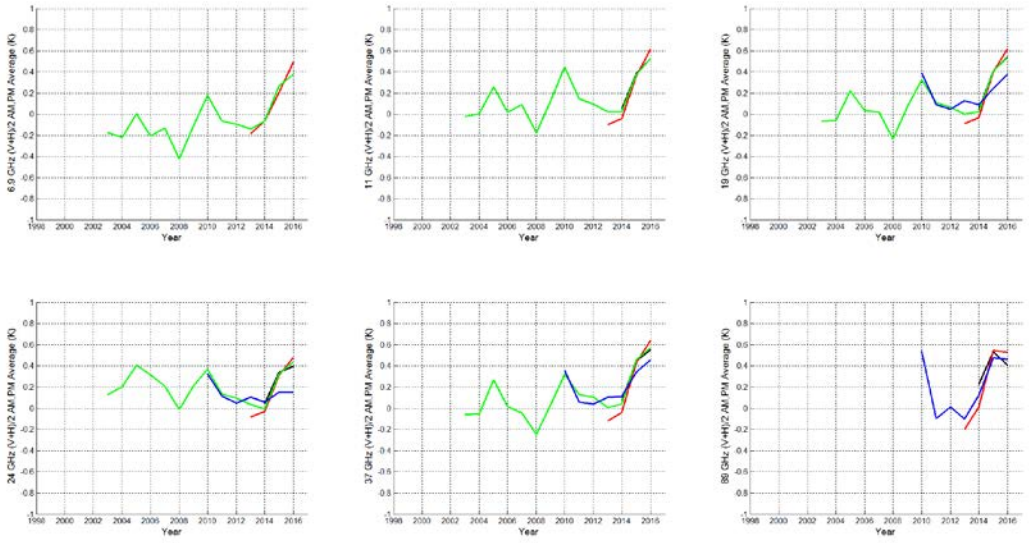

Figure 2. Comparison of AMSR-2 (red), GMI (black), WindSat (green), and F18 SSM/IS (blue) over the Amazon Rainforest. For all sensors, we show the difference between the brightness temperature (T_B) measurement minus the T_B model derived from NASA's precisely calibrated GMI sensor. The T_B value is the average of v-pol and h-pol. Also day and night observations have been averaged. All sensors show similar year-to-year variations, and this fact indicates the year-to-year variations seen in this figure are due to actual changes in the microwave emission from the Amazon rainforest rather than sensor calibration errors.

Absolute Calibration

As previously discussed, the antenna temperature is a measure of radiant power entering the feedhorn. It is the brightness temperature of the surrounding environment integrated over the gain pattern of the SSM/I parabolic reflector and feedhorn assembly. This integration can be well approximated by [*Wentz*, 1991]

$$T_{Ai} = q_i T_{Bi} + \chi_i q_i T_{Bj} + \eta_i T_{c,plk} \tag{23}$$

$$q_i = \frac{1-\eta_i}{1+\chi_i} \tag{24}$$

where the spillover η is the fraction of received power coming from cold space and the cross polarization coupling χ is fractional power coming from the orthogonal polarization. The subscript *i* denotes polarization: *i* = *v* or *h*, and the subscript *j* denotes the orthogonal polarization. When *i* = *v*, then *j* = *h*, and when *i* = *h*, then j = *v*. $T_{c,plk}$ is the Planck-adjusted value of cold space given in Section 3.4.3. The inverse of this relationship is called the antenna pattern correction (APC) and is given by

$$T_{Bi} = \frac{q_j T_{Ai} - \chi_i q_i T_{Aj} + \left(\chi_i q_i \eta_j - q_j \eta_i\right) T_{c,plk}}{q_i q_j \left(1-\chi_i \chi_j\right)} \tag{25}$$

In the more abbreviated notation used by equation (1) and (2), we let the antenna function $\Gamma(\mathbf{T_B})$ denote the conversion of T_B to T_A for all 7 radiometer channels, and likewise $\Gamma^{-1}(\mathbf{T_A})$ is the APC function for all channels.

There is no 22 GHz h-pol T_A measurement for SSM/I or SSMIS, and hence (25) cannot be used to find the 22 GHz T_B. To avoid this problem, the input to the geophysical retrieval algorithm is T_A rather than T_B, and the calibration is also done in terms of T_A rather than T_B, as discussed in Section 3.4.1. This avoids having to convert the single-pol 22 GHz T_A into a T_B.

Absolute calibration of the SSM/I or SSMIS T_A measurements to the RTM as dictated by (11) can be obtained by varying η and χ so that the mission averaged T_A measurements agree with RTM. Since there are two unknowns (η and χ) for each channel, the estimation must be constrained in some way. We make the assumption that η and χ are the same for both polarizations:

$$\begin{aligned} \eta_v &= \eta_h \\ \chi_v &= \chi_h \end{aligned} \tag{26}$$

For the dual polarization channels, the constraint imposed by (26) results in two unknowns for each polarization pair. The parameters η and χ are then varied to satisfy equation (11) for both polarizations.

At 22 GHz for which there is only the v-pol measurement, we need to employ an additional constraint to find both η and χ. The vapor retrievals for the F13 SSM/I are compared to collocated and validated WindSat vapor retrievals. The validation of the WindSat vapor retrievals is based on comparisons with GPS values, and these comparisons show good, unbiased agreement over the full range of water vapor from 0 to 65 mm. The vapor retrievals are driven by the 22-GHz measurements, and the 0 to 65 mm range corresponds to a range in the 22V T_A of about 75 K. This provides enough dynamic range to estimate both the offset and the slope of the SSM/I minus WindSat vapor difference. The parameters η and χ are found so as to make the SSM/I vapor retrievals agree with Windsat while satisfying equation (11). These two constraints then provide the means for finding both η and χ at 22 GHz. The value found for χ is 0.01560 as compared to the pre-launch value of 0.00983. This is a small change, equivalent to about 0.3 K in T_A. Rather than trying to do this type of analysis for each SSM/I, we simply use χ_{22v}=0.01560 for all SSM/Is and SSMIS. Having fixed χ_{22v}, then η_{22v} becomes the single parameter used to satisfy equation (11) for the other SSM/Is.

Assumption (26) that the spillover and polarization coupling is the same for both polarizations is supported by both pre-launch antenna pattern measurements and on-orbit SSM/I observations of heavily forested areas. *Hollinger et al.* [1987] report the same F08 SSM/I pre-launch spillover values for v-pol and h-pol. The reported polarization difference in χ ranged from 0.0006 to 0.005 (equivalent to about 0.05-0.25 K in T_A). Pre-launch antenna measurements of the other SSM/Is also indicate little polarization difference for η and χ [*Colton and Poe*, 1999].

The other evidence that supports (26) is the SSM/I observations of heavily forested areas where the v-pol and h-pol T_B are nearly the same. Setting $T_{Bv} = T_{Bh}$ in (23) gives

$$T_{Ai} = (1-\eta_i)T_B + \eta_i T_{c,plk} \qquad (27)$$

Analysis of the SSMIS T_A observations of these heavily forested areas shows little if any polarization difference. Hence according to (27), this implies $\eta_v = \eta_h$.

Table 4 give the spillover and polarization coupling for the SSMIS F18.. These values are from the final step in the calibration process that minimizes both $\mathbf{\delta E_p}(i, j)$ and $T_A - T_{A,rtm}$, as discussed in Section 3.4.2.

It should be noted that an error in η and an error in the hot target temperature T_h have nearly the same effect on the calculation of T_B. They both introduce a multiplicative bias in T_B. The 1 K reduction of the hot target temperature as given by the thermistors (see Section 4) results in our derived spillover values shown in Table 3 and Figure 2 being 0.004 higher. As Figure 2 shows, this increase in η results in slightly better agreement with the pre-launch values when considering all SSM/Is and all frequencies. We have observed the same phenomenon with AMSR-E, WindSat, and SSM/IS: decreasing the thermistor T_h by 1 K results in spillover values that better agree with pre-launch measurements. Whether this is real (i.e, the effective temperature of the hot target is

indeed a little less than the thermistor value) is difficult to say for sure. In any event, for nearly all applications it does not matter whether you assign this small error to η or T_h.

Table 3. Spillover (η) and Polarization Coupling (χ) F18 SSMIS

	19V	19Hz	22V	37V	37H	92V	92H
η	0.03265	0.03268	0.01940	0.0170	0.016950	0.03264	0.03446
χ	0.01710	0.01710	0.015084	0.22618	0.02618	0.00930	0.00930

Along-Scan Correction

One of the first SSM/I calibration problems that was detected was an along-scan error [*Wentz*, 1991]. Towards the end of the Earth scan, the cold target mirror begins to intrude into the field of view of the feedhorn. As a result, the T_A measurements exhibit a systematic roll-off of about 1 K at the end of the scan. Our model for the along-scan error is to assume the radiation entering the feedhorn is a combination of Earth radiation $T_{A,earth}$ reflected off the parabolic antenna and cold space radiation $T_{c,plk}$ reflected off the cold target mirror:

$$T_{A0} = \left[1-\mu(\omega)\right]T_{A,earth} + \mu(\omega)T_{c,plk} \tag{28}$$

where $\mu(\omega)$ is a function of the along-scan position ω. Since $T_{A,earth}$ is the desired quantity, the required adjustment according to (12) and (28) is

$$\Delta T_{A,\omega} = \frac{-\mu(\omega)}{1-\mu(\omega)}\left(T_{A0} - T_{c,plk}\right) \tag{29}$$

Of the five relative T_A adjustments, the derivation of along-scan correction $\Delta T_{A,\omega}$ is probably the most straightforward and provides a good example of how inter-satellite T_A differences are used for the derivation. In this case we use the inter-satellite T_A differences $\delta T_A(i, j)$ defined by (14). $\mu(\omega)$ for F18 was determined via comparison with GMI. $\delta T_A(i, j)$ represent millions of collocated sensor-i minus sensor-j T_A differences. As discussed in Section 1.8.2, when computing $\delta T_A(i, j)$ all adjustments are applied other than the $\Delta T_{A,\omega}$ currently under consideration. Thus the assumption can be made that $\delta T_A(i, j)$ equals $\Delta T_{A,\omega}$. This assumption becomes more rigorous as the calibration procedure iterates and the various adjustments converged. Assuming $\delta T_A(i, j) = \Delta T_{A,\omega}$ and inverting (29) to yield $\mu(\omega)$ gives

$$\mu(\omega) = \frac{\delta T_A(i, j)}{\delta T_A(i, j) - \left(T_{A0} - T_{c,plk}\right)} \tag{30}$$

There are 64 scan positions for the 19-37 GHz channels and 128 positions for 85 GHz. Averages of μ(*ω*) are found for each scan position thereby creating μ(*ω*) tables. Figure 3 shows the μ(*ω*) tables for SSMIS for all channels..

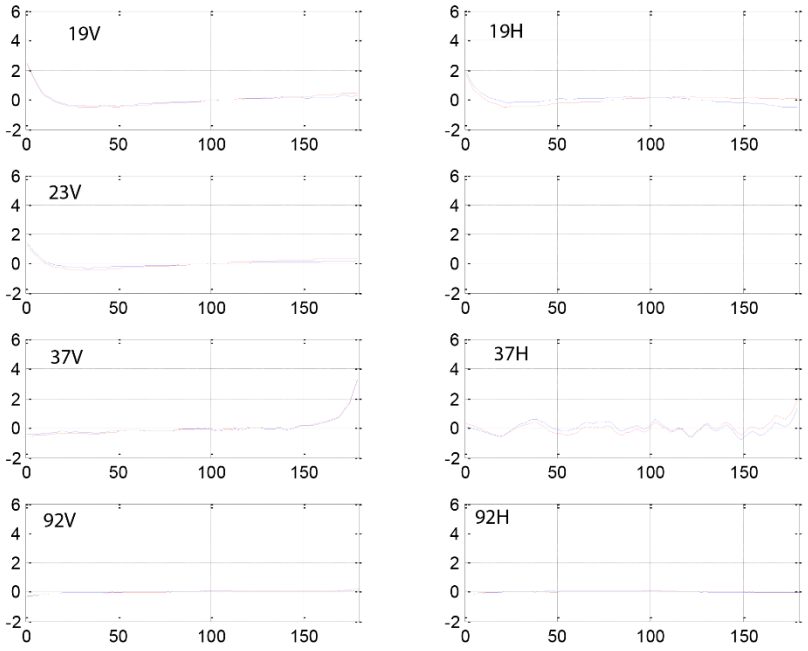

Figure 3. The along-scan correction that is applied to the SSMIS F18 T_A. To show these results in terms of a value indicative of the T_A adjustment, μ(*ω*) has been multiplied by 200 K. The adjustment has the effect of increasing T_A at the ends of the scan to compensate for the intrusion of the cold mirror into the field of view. The 2 colors correspond ascending and descending nodes.

Adjustments to the Hot Target Temperature

As discussed in Section 3.4.3, the specification of the hot target temperature T_h is problematic. One must infer T_h from thermistor readings attached to the hot target. However, there will be some error in using these readings to estimate the effective emission temperature of the hot target. For example, the SSM/I has only 3 thermistors, and thermal gradients, both horizontal and vertical, over the extent of the hot target will

introduce error. Such problems have been reported for both WindSat and the F16 SSM/IS [*Twarog et al*., 2006; *Sun and Weng*, 2008]. Herein, we find a similar, but smaller, problem for the F18 SSMIS.

The hot target temperature adjustment is found in a way analogous to that described in Section 3.4.5 for the along-scan correction. The change to T_A due to an error ΔT_h in specifying the hot target temperature is given by

$$\Delta T_{A,ht} = \frac{T_A - T_c}{T_h - T_c} \Delta T_h \tag{31}$$

This is equivalent to adding ΔT_h to T_h in equation (19). Following the procedure described in Section 3.4.5, the assumption is made that $\delta T_A(i, j) = \Delta T_{A,ht}$ and (31) is inverted to yield ΔT_h.

$$\Delta T_h = \frac{T_h - T_c}{T_A - T_c} \delta T_A(i, j) \tag{32}$$

To obtain a more robust estimate for ΔT_h, the assumption is made that ΔT_h is polarization independent (i.e., same for v-pol and h-pol). There is good physical and empirical justification for this assumption. Assuming ΔT_h is independent of polarization allows the usage the following linear combination of v-pol and h-pol T_A differences:

$$\delta T_{Ax}(i, j) = \delta T_{Av}(i, j) - \kappa \delta T_{Ah}(i, j) \tag{33}$$

where the weighting coefficient $\kappa = 0.53$. This linear combination is selected because it is very insensitive to variations in the atmosphere moisture (i.e., V and L). Over the oceans, changes in atmospheric absorption due to either V or L affect h-pol about twice as much as v-pol, and hence $\delta T_{Ax}(i, j)$ is largely insensitive to these changes. The largest source of error in computing $\delta T_A(i, j)$ is the specification of V and L for $\mathbf{T}_{A,rtm}(j)$, and using (33) greatly reduces this error. Combining (32) and (33) gives

$$\Delta T_h = \frac{(T_h - T_c)\delta T_{Ax}(i, j)}{T_{Av} - T_c - \kappa(T_{Ah} - T_c)} \tag{34}$$

Equation (34) cannot be used for the 22 GHz channel because there is only a v-pol measurement. For this case, we use the 19 GHz ΔT_h to specify the 22 GHz value.

Analyses of hot target errors for WindSat [*Twarog et al*., 2006] and SSM/IS [*Sun and Weng*, 2008] indicate that at certain points in the orbit the sun shining on the hot target produces thermal gradients that are not captured by the thermistors. These events are typically characterized as 'solar intrusions' where the solar radiation either directly or via a reflection impinges onto the hot target. For these events the effective temperature of the hot target is not adequately represented by $T_{h,therm}$. The geometry of the solar intrusions can be complex with both direct and reflected intrusions causing problems. For the SSM/Is, rather than trying to explicitly model the geometry of the intrusions, we

simply assume ΔT_h is a function of the sun's azimuth angle α and polar angle β as measured in the spacecraft coordinate system for which the z-axis points up away from nadir and the x-axis is the spacecraft velocity vector. We denote this function by $\Delta T_h(\alpha, \beta)$. Equation (34) is then used to make tables of $\Delta T_h(\alpha, \beta)$. The derivation of $\Delta T_h(\alpha, \beta)$ requires a pair of collocated imaging radiometers, in this case GMI and SSMIS F18.

In addition to $\Delta T_h(\alpha, \beta)$, there is a second adjustment that is made to the hot target temperature. This adjustment, which is applied to all SSM/Is, is based on the difference between the evening (pm) and morning (am) T_A measurements, and is denoted by $\Delta T_h(\psi, t)$, where ψ is the spacecraft angular position in orbit and t is time. The angle ψ equals 0 when the spacecraft is at its southern-most position in the orbit. This adjustment is modeled by a small but very systematic error we see between the pm and am measurements that we do not believe is due to real diurnal effects. The $\Delta T_h(\psi, t)$ adjustment is quite small, typically being ±0.2 K, and never exceeds ±0.5 K except at the very end of the missions for F10 and F15. The adjustment takes the form

$$\Delta T_h(\psi, t) = \left[G_0 + G_1(t) + G_{85}(t_{asc}) \right] \sin\psi \qquad (35)$$

where G_0 is a constant that just depends on channel number and $G_1(t)$ is a slowly varying function of time t that is independent of channel number. The last term $G_{85}(t_{asc})$ is a special adjustment only applied to the 85 GHz channels. The derivation of these three terms and an explanation of how they are separated from the natural diurnal variation of $\mathbf{E_p}$ is given in Section 3.4.12.

The two hot target adjustments are then added together to obtain the total correction:

$$\Delta T_h = \Delta T_h(\alpha, \beta) + \Delta T_h(\psi, t) \qquad (36)$$

Figure 4 shows the Adjustments made to the hot load temperature for F18.

3.4.1 Physical and Mathematical Description

The output of a microwave (MW) radiometer is a voltage that is converted to integer counts for the telemetry downlink. The first step of the calibration process is to convert these voltage counts to an antenna temperature T_A, which is discussed in Section 3.4.3. By definition, T_A is a measure of radiant power entering the feedhorn. It is the brightness temperature (T_B) of the surrounding environment integrated over the gain pattern of the SSM/I parabolic reflector and feedhorn assembly. In orbit, about ¾ of the surrounding environment consists of cold space at a temperature near 2.7 K, and the remaining ¼ is the Earth, which has a brightness temperature T_B between 100 and 300 K, depending on the scene. Thus, the antenna temperature is biased low relative to the Earth T_B, and this is called the spillover effect. In addition, some Earth scenes are very polarized, particularly the oceans, and the anten

na gain pattern tends to mix polarizations. As a result, the antenna temperature is not as polarized as the Earth T_B, and this is called the cross polarization coupling effect. Section 3.4.4 expresses the relationship between T_A and T_B as

$$\mathbf{T_A} = \Gamma(\mathbf{T_B}) \qquad (1)$$

where $\mathbf{T_B}$ and $\mathbf{T_A}$ are the brightness temperatures and antenna temperatures for the 7 SSM/I or SSMIS channels. Herein, we use **boldface** to denote the array containing the full channel set of values. When expressed in non-boldface, it is the same quantity but for a single channel. The antenna function Γ depends on the antenna spillover η and cross polarization coupling χ, as definded in Section 3.4.4. The inverse of this relationship is called the antenna pattern correction (APC) and provides the means to retrieve brightness temperature values from the T_A measurements:

$$\mathbf{T_B} = \Gamma^{-1}(\mathbf{T_A}) \qquad (2)$$

The calibration process is done in terms of T_A rather than T_B because the former is the more fundamental measurement. A T_B value is a mixture of two SSM/I channels, and working in terms of T_B would make it more difficult to separate calibration problems coming from different channels. There are other reasons for doing the calibration in terms of T_A which as discussed later.

The Version-7 calibration is heavily based on RSS most recent ocean radiative transfer model (RTM), which is also called V8. The basics of the ocean RTM are described by *Wentz* [1997] and *Wentz and Meissner* [2000]. More recent updates include *Meissner and Wentz* [2002, 2003, 2004, 2012]. The most recent versions are described in Meissner and Wentz [2012] (for the surface emissivity) and Wentz and Meissner [2016] (for the atmosphere) [2016]. Since 2016, we have made a small adjustment to the water vapor line as part of the V8 calibration study. The full RTM described in these two pulbications involves an radiative emissive and scattering rough ocean surface along with vertical integrations through the atmosphere. It has been shown that the full RTM is well represented by a simplified RTM, which herein we denote by the function Ψ:

$$\mathbf{T}_{\mathbf{B,rtm}} = \Psi\left(\mathbf{E}_{\mathbf{p}}\right) \quad (3)$$

$$\mathbf{T}_{\mathbf{A,rtm}} = \Gamma\left[\Psi\left(\mathbf{E}_{\mathbf{p}}\right)\right] \quad (4)$$

$$\mathbf{E}_{\mathbf{p}} = \left[T_s, W, \phi_w, V, L\right] \quad (5)$$

where $\mathbf{T_{B,rtm}}$ and $\mathbf{T_{A,rtm}}$ are the TOA T_B and T_A corresponding to the 7 channels. The set of environmental paramters ($\mathbf{E_p}$) includes sea-surface temperatue (T_s), sea-surface wind speed and direction (W, ϕ_w), columnar water vapor (V), and columnar liquid cloud water (L). Rain need not be considered because we exclude area of rain when doing the calibration. There are also secondary dependences such as the shape of the vapor and cloud vertical profiles in conjunction with the atmospheric temperature profile. The function $\Psi(\mathbf{E_p})$ is derived so that the effect of these secondary dependences when averaged globally over monthly time scale goes to zero. Implicit in (3) and (4) are the sensor parameters including the incidence and azimuth viewing angles θ_i and ϕ_i and the observation frequency.

In an important sense, the retrieval algorithm is the inverse of the RTM. For the retrieval algorithm, the inputs are either T_B or T_A measurements, and the output is the environmental parameters. We let Ψ^{-1} denote the retrieval algorithm while acknowledging that it is not a simple mathematical inverse of the RTM Ψ. For SSM/I and SSMIS, there is not enough orthogonal sensitivity in its 7 channels to retrieve T_s and ϕ_w, and these two parameters are treated as *a priori* arguments coming from NCEP fields. Thus the retrieval algorithm is denoted by

$$\mathbf{E}_{\mathbf{p}} = \Psi^{-1}\left[\mathbf{T}_{\mathbf{A}} \,|\, T_s, \phi_w; \eta, \chi\right] \quad (6)$$

where $\mathbf{T_A}$ denotes the input set of antenna temperatures for the different SSM/I channels. Formulating the retrieval algorithm in term of T_A rather than T_B requires that η and χ also be included as additional *a priori* arguments, and the retrieval algorithm is trained using simulated T_As rather than T_Bs. Our motivation for using a T_A-based retrieval algorithm is discussed in Section 3.4.4.

The degree to which the retrieval algorithm is a functional inverse of the RTM is determined by computing closure. This is done by inputting the three retrievals (W, V, L) into the RTM to predict the 7 SSM/I T_As. This closure calculation is represented by

$$\mathbf{T}_{\mathbf{A,rtm}} = \Gamma\left\{\Psi\left\{\Psi^{-1}\left[\mathbf{T}_{\mathbf{A}} \,|\, T_s, \phi_w; \eta, \chi\right]\right\}\right\} \quad (7)$$

and the degree of closure is measured by the difference between the RTM T_A minus the measurement T_A:

$$\boldsymbol{\delta}\mathbf{T}_{\mathbf{A,closure}} = \mathbf{T}_{\mathbf{A}} - \mathbf{T}_{\mathbf{A,rtm}} \quad (8)$$

There is no guarantee that one can precisely recover the 7 T_As given just 3 retrievals. Deficiencies in the RTM and/or retrieval algorithm along with calibration errors in the T_As will all degrade the closure. We will show that at this point in our development cycle the

deficiencies in the RTM and retrieval algorithm are quite small, and $\mathbf{\delta T_{A,closure}}$ is mostly an indicator of calibration errors remaining in the T_A measurements. When calibration errors are removed, $\mathbf{\delta T_{A,closure}}$ is typical 0.1-0.2 K or less when averaged regionally over weekly time scales (see Figure 6 below). This high precision in closure allows us to achieve absolute calibration and inter-satellite calibration both in terms of $\mathbf{T_A}$ and $\mathbf{E_p}$ simultaneously.

Much of the calibration work is based on comparisons between the T_A measurements and $\mathbf{T_{A,rtm}}$. In addition, we use direct comparisons of T_A measurements. When directly comparing T_A measurements, it is necessary to normalize the measurements to a common incidence angle and antenna function Γ (i.e., common η and χ). In addition, since the azimuth viewing angles ϕ_i may be different for the two observations, the effect of wind direction on the observations needs to be removed. This normalization is done by first converting the T_A measurement to a brightness temperature using (2). The brightness temperature is then normalized as follows:

$$\mathbf{T'_B} = \mathbf{T_B} - \Psi\left(T_s, W, \phi_w, V, L; \theta_i\right) + \Psi\left(T_s, W, \cdots, V, L; \theta_{io}\right) \qquad (9)$$

where the prime sign denotes normalization, θ_i is the actual incidence angle of the observation, and θ_{io}=53.25° is the common incidence angle to which all SSM/I observations are normalized. The time series plot of θ_i in the Appendix show that θ_i is usually within ±0.5° of θ_{io}. The second Ψ function in (9) is called the isotropic RTM for which the wind direction dependence is set to zero. The normalized brightness temperature is then converted back to an antenna temperature. For this conversion back to T_A, a common spillover η and cross-pol coupling χ are used for all 6 SSM/Is. We use the F13 η, χ values. The normalized T_A is then given by

$$\mathbf{T'_A} = \Gamma_{F13}\left(\mathbf{T'_B}\right) \qquad (10)$$

3.4.2 Data Merging Strategy

Not applicable.

3.4.3 Numerical Strategy

All calculation in the algorithm are straightforward adjustments using look-up tables and simple algebraic expressions. Most calculations are performed using 4 byte reals. The exception is geolocation calculations, which sometimes requires 8-byte precision.

3.4.4 Calculations

The first step in the calibration is to determine the antenna spillover η and cross polarization coupling χ, thereby establishing the absolute calibration of the SSM/I brightness temperatures. A prerequisite is to require that the $\mathbf{E_p}$ retrievals agree with *in situ* observation in an unbiased sense. The absolute calibration of wind speed is determined from anemometers on moored buoys that are part of the NDBC, TAO, TRITON, and PIRATA arrays. Water vapor absolute calibration is based on radiosonde and GPS measurements. For liquid cloud water, there are no *in situ* measurements extensive and

accurate enough to meet our requirements. In this case, we use a statistical histogram method based on the fact that a significant portion of the SSM/I measurements will be free of clouds. This fact established a well determined zero-point for a histogram of cloud water. See *Wentz* [1997] for details. The absolute calibration criterion then requires that the mission-averaged T_A equals the RTM T_A

$$\left\langle \mathbf{T}_\mathbf{A} \right\rangle = \left\langle \mathbf{T}_{\mathbf{A,rtm}} \right\rangle \equiv \left\langle \Gamma\left[\Psi\left(\mathbf{E}_\mathbf{p} \right) \right] \right\rangle \tag{11}$$

where the brackets denote an average over the entire mission of a specified SSM/I or SSMIS. The antenna parameters η and χ, which are the implicit arguments of Γ, are then adjusted to satisfy the equality, as is described in Section 3.4.4. Early on in the calibration process, $\mathbf{E_p}$ comes from earlier versions of SSM/I or SSMIS processing and from other collocated satellites like WindSat. As the calibration process converges, $\mathbf{E_p}$ is the retrievals from the particular SSM/I or SSMIS being calibrated. Hence, a second instrument is not required by (11). The only requirement is that $\mathbf{E_p}$ is unbiased relative to the *in situ* observations. A final, small adjustment to η and χ is done at the end of the calibration procedure to ensure precise inter-satellite agreement of the geophysical retrievals, as is discussed later in this section.

The second step in the calibration is to find the relative calibration errors $\mathbf{\Delta T_A}$ for the 7 channels. These errors are subtracted from $\mathbf{T_{A0}}$, which is the T_A measurement derived from the radiometer counts given by (19) in Section 3.4.3, in order to obtained the 'true' antenna temperature $\mathbf{T_A}$:

$$\mathbf{T}_\mathbf{A} = \mathbf{T}_{\mathbf{A}0} - \mathbf{\Delta T}_\mathbf{A} \tag{12}$$

The relative errors depends on a number of parameters such as scan position, solar angles, position in orbit, etc., and these are listed later in this section. A given relative error is derived so that its mission average is near zero:

$$\left\langle \mathbf{\Delta T}_\mathbf{A} \right\rangle \approx 0 \tag{13}$$

In practice, the mission-average relative error will have a small bias depending on the details of how the mission-average is done, but in general the bias is less than 0.1 K, which is much smaller than the biasing due to the adjustments made to the antenna spillover and coupling. So the η, χ adjustment drives the absolute calibration.

Two types of T_A inter-comparisons are done as represented by the following equations.

$$\mathbf{\delta T}_\mathbf{A}(i,j) = \mathbf{T}_\mathbf{A}(i) - \mathbf{T}_{\mathbf{A,rtm}}(j) \tag{14}$$

$$\mathbf{\delta T}'_\mathbf{A}(i,j) = \mathbf{T}'_\mathbf{A}(i) - \mathbf{T}'_\mathbf{A}(j) \tag{15}$$

where we have introduced the indices *i* and *j* as arguments to denote a pair of collocated radiometer measurements. The first type of comparison (14) is between the T_A

measurement of one radiometer versus the RTM T_A predicted using the E_p retrievals from a second instrument. The second type of comparison (15) is the same as the first, except that the T_A measurements are first normalized to a common incidence angle and common η and χ. In addition, the normalization also removes the effect of wind direction. This normalization, which is denoted by the prime symbol, is accomplished by equations (9) and (10) and is intended to make the T_A measurements from two imaging radiometers directly comparable. For the first type of inter-comparison, the collocation criterion is based on daily, ¼° latitude/longitude maps. Separate maps are made for the ascending and descending orbit segments. The collocation criterion is that for a given map, a ¼° cell must contain observations from both instruments. The collocation criterion is the same for the second type of inter-comparison except the maps are 5-day (pentad), 1° latitude/longitude maps. For V8 processing, all calibration is based on comparison with either the GPM microwave imager (GMI) or the TRMM microwave imager (TMI). Because these two instruments are in rapidly precessing orbits, they are closely collocated in time with any polar orbiter fairly often, and a collocation dataset with the time distance clustered around zero difference can be constructed, minimizing problems due to any diurnal cycle present.

We consider the most important scientific criterion for inter-satellite calibration is that the collocated geophysical retrievals from pairs of SSM/Is precisely agree. This is particularly important when constructing multi-decadal time series from the 25 years of SSM/I observations. Thus as the final step in the calibration procedure, we require the wind, vapor, and cloud retrievals from the pairs of SSM/I to precisely agree. In this case, the inter-satellite comparison is represented by

$$\mathbf{\delta E_p}(i,j) = \mathbf{E_p}(i) - \mathbf{E_p}(j) \qquad (16)$$

The $\mathbf{\delta E_p}(i,j)$ differences for the 7 primary overlaps are minimized by making small adjustments to the antenna parameters η and χ. Adjustments to η and χ produce changes in the retrievals as indicated by (6). While minimizing $\mathbf{\delta E_p}(i,j)$, we continue to required that (11) is satisfied as closely as possible. Imposing these two constraints simultaneously (i.e., the minimization of $\mathbf{\delta E_p}(i,j)$ and the T_A agreement with the RTM) provides the final values for η and χ. When averaged over the overlap periods, the procedure minimizes the inter-satellite wind and vapor differences to about 0.01 m/s and 0.01 mm. After accounting for diurnal variation, inter-satellite cloud differences are minimized to 0.0002 mm. In addition, the mission averaged T_A minus $T_{A,rtm}$ differences are typically 0.05 K.

There are 5 kinds of relative T_A adjustments:

$$\mathbf{\Delta T_A} = \mathbf{\Delta T_{A,\omega}} + \mathbf{\Delta T_{A,ht}} + \mathbf{\Delta T_{A,isat}} + \mathbf{\Delta T_{A,drift}} + \mathbf{\Delta T_{A,tf}} \equiv \sum_{k=1}^{5} \mathbf{\Delta T_{A,k}} \qquad (17)$$

where:

$\mathbf{\Delta T_{A,\omega}}$ is the along-scan adjustment (Section 3.4.5)

$\mathbf{\Delta T_{A,ht}}$ is the adjustment to the hot target temperature (Section 3.4.6)

$\mathbf{\Delta T_{A,isat}}$ is an adjustment that is unique and specific for the F08, F10, and F15 SSM/I (Sections 3.4.7, 3.4.8, and 3.4.9)

$\mathbf{\Delta T_{A,drift}}$ is a small drift correction applied to F11 and F13 SSM/I (Section 3.4.10)

$\mathbf{\Delta T_{A,tf}}$ is the 'target factor' adjustment (Section 3.4.11)

These adjustments are found so as to minimize either $\mathbf{\delta T_A}(i, j)$ or $\mathbf{\delta T'_A}(i, j)$ as is explained in the subsequent sections.

The adjustments are derived one at a time. Once a given adjustment is found, it is applied to the T_A measurement, and then the next adjustment is found. Once all adjustments are found, we repeat the procedure and find residual adjustments. The residual adjustments are very small (i.e., we get nearly the same adjustment the second time around). For example according to this procedure, when equation (14) to find the n^{th} adjustment $\mathbf{\Delta T_{A,n}}$, the value of $\mathbf{T_A}$ in (14) is

$$\mathbf{T_A} = \mathbf{T_{A0}} - \sum_{k \neq n} \mathbf{\Delta T_{A,k}} \qquad (18)$$

which says that all adjustments other than the adjustment currently being derived are applied to $\mathbf{T_{A0}}$. The same holds true when equation (15) is being used to derive the adjustment.

Using inter-satellite comparisons to find the $\mathbf{\Delta T_A}$ risks the possibility of calibration errors from one sensor aliasing into another. We call this sensor error crosstalk. To assess this problem, we experimented with many variations of the calibration procedure presented here, such as using different pairs of SSM/Is to derive the same adjustments. For most types of errors, sensor error crosstalk does not appear to be a problem. As an example, when finding the along-scan adjustment $\mathbf{\Delta T_{A,\omega}}$, a given along-scan cell position for the first SSM/I will tend to randomly collocate with all the cell positions for the second SSM/I. As a result, the ω-errors in the first SSM/I do not alias into $\mathbf{\Delta T_{A,\omega}}$ for the second SSM/I. Furthermore, on the second iteration of the calibration procedure, the errors in the reference SSM/I are mostly removed. The one case where sensor error crosstalk is of concern is the F13 time drift, which is discussed in Section 3.4.10.

Another question on the robustness of the calibration procedure is the orthogonality of the 5 adjustments. Can a given calibration error be represented by more than one type of adjustment? The 5 types of adjustments have been designed to be dissimilar so as avoid this problem. Also, we have gone through many iterations of the calibration process, and the order of finding the 5 adjustments did not seem to really matter as long as two complete iterations of all 5 adjustments is done. Furthermore, any creeping of a calibration error from one type of adjustment to another has little effect on the overall calibration because the adjustments are added together. The only possible problem is the interpretation of the individual errors sources may be a bit skewed.

A useful calibration tool is the degree of closure as expressed by (8), or equivalently by (14) with $i = j$. It would be very convenient if $\mathbf{\delta T_{A,closure}}$ could be used to infer the T_A adjustments because one would then not need to rely on collocations with another SSM/I. However, if the $\mathbf{E_P}$ from the same satellite to compute $\mathbf{T_{A,rtm}}$, then the errors in $\mathbf{E_p}$ due to calibration errors $\mathbf{\Delta T_A}$ would be highly correlated with $\mathbf{\Delta T_A}$, and this correlation would tend to hide and/or distort the derivation of $\mathbf{\Delta T_A}$. This is why we use the $\mathbf{E_P}$ from a different SSM/I to compute $\mathbf{T_{A,rtm}}$. The E_p errors from a second SSM/I are much less correlated with the $\mathbf{\Delta T_A}$ errors of the first SSM/I. That is not to say $\mathbf{\delta T_{A,closure}}$ is not useful. In fact, it is an extremely useful tool for verification and diagnosing residual calibration error as is shown in Section 3.4.7 for the F08 SSM/I. The diagnostic $\mathbf{\delta T_{A,closure}}$ is best used as a final step after all known calibration errors are removed.

Unadjusted Antenna Temperature

In computing the unadjusted SSM/I antenna temperature, the basic assumption is that the radiometer output voltage expressed as counts is linearly related to the input power at the feedhorn expressed as T_A, with a small quadratic adjustment. Under these assumptions, the unadjusted antenna temperature is

$$T_{A0} = \frac{(T_h - T_c)C_e + T_c C_h - T_h C_c}{C_h - C_c} \qquad (19)$$

where the subscript *0* denotes no adjustments have been made. The terms C_c, C_h, and C_e are the radiometer counts when the radiometer is looking at the cold calibration target, the hot calibration target, and the earth scene, respectively. The temperatures T_c and T_h are the effective temperatures of the cold and hot calibration targets. Equation (19) is simply expressing the assumption that the radiometer counts vary linearly as the scene temperature varies from T_c to T_h.

The first difficulty in the calibration process is accurately specifying T_c and T_h. For example, the cold target is a mirror pointing towards cold space, which has a temperature of 2.73 K (i.e., the cosmic background temperature). However, if the mirror is not a perfect reflector or if the mirror is receiving some radiation from other sources such as the spacecraft or the Earth, the true value for T_c will be greater than 2.73 K. The specification of T_h is even more difficult. In this case, one must infer T_h from thermistor readings attached to the hot target. There will be some error in using these readings to estimate the effective emission temperature of the hot target. For example, thermal gradients, both horizontal and vertical, over the extent of the hot target will cause problems. SSM/I has only 3 thermistors attached to the hot target.

Our specification of the cold target temperature is

$$T_c = T_{c,plk} + \delta T_c \qquad (20)$$

The first term $T_{c,plk}$ is the Planck-adjusted value of cold space. The relationship between radiation intensity and temperature is given by Planck's law. In the lower microwave

spectrum, this relationship is nearly linear and the Rayleigh-Jeans approximation is used. However as the frequency increases, the Rayleigh-Jeans approximation begins to break down. This effect can be compensated for by adjusting the cold space temperature. By doing this, one can continue to assume a linear relationship between radiation and temperature. This is standard practice and the value for $T_{c,plk}$ is 2.752, 2.761, 2.822, and 3.203 K for the four SSM/I frequencies (19, 22, 37, and 85 GHz). The second term δT_c is a small offset we apply to account for radiation coming from sources other than cold space such as the spacecraft and Earth. A value of δT_c = 0.3 K is used for all channels and all SSM/Is. This value assumes 0.2% of the radiation comes from the spacecraft and earth, which have a typical temperature of 150 K. We know the effective temperature of the cold target must be higher than cold space, and the inclusion of δT_c is a small hedge for this. We use this 0.3 K offset for all satellite MW imagers including AMSR-E, WindSat, TMI, and SSM/IS.

Our specification of the hot target temperature is

$$T_h = T_{h,therm} + \delta T_h \tag{21}$$

The first term $T_{h,therm}$ is the hot target temperature derived just from the thermistors measurements, and the second term δT_h is a small offset we apply to account for an overall bias in the effective hot target temperature. A value of δT_h = −1.0 K is used for all channels and all SSM/Is. The inclusion of δT_h results in slightly better agreement between the antenna spillover values derived herein and pre-launch values, as is discussed in Section 5. $T_{h,therm}$ is given by

$$T_{h,therm} = t_h + \xi\left(t_p - t_h\right) \tag{22}$$

The temperature t_h is the average of the 3 thermistor readings attached to the hot target and the temperature t_p is the reading from the single thermistor on the SSM/I drum plate facing the hot target. The coefficient ξ is a value derived from prelaunch thermal-vacuum measurements, and its value is 0.01 [*Hollinger et al.*, 1987]. Equation (22) is saying 99% of the hot target radiation is coming from the hot target itself and 1% of the radiation is coming from the reflection of the drum face off the hot target. For the F13 SSM/I, only hot-target thermistor 2 is used for t_h because the other 2 thermistors displayed considerable noise [*Colton and Poe*, 1999].

Noise in C_c and C_h is reduced by averaging measurements from adjacent scans. We use a time window of ±12 seconds centered on the scan being processed. If there are no data gaps, this time window will include 13 scans. For the 19-37 GHz channels, calibration counts are only collected every other scan. For 85 GHz, calibration counts are collected every scan. For each scan, 5 calibration measurements are taken of the cold target and another 5 for the hot target. Thus our ±12 seconds time window provides 35 cold counts and 35 hot counts for each of the lower-frequency channels and 65 counts at 85 GHz. This is a sufficient number of samples to reduce the noise in the calibration counts to an acceptable level.

In a second step, a small non-linearity correction is applied to T_A.

$$T_A = T_{A0} - 4\lambda X\left(1 - X\right), X = \frac{\left(T_A - T_c\right)}{T_h - T_c}$$

Here, λ is the maximum difference from the linear result, which occurs for T_{A0} values halfway between T_h and T_c. The values for X for each of the 7 channels for F18 are shown in the Table 2

Table 4. Values of the non-linearity adjustment parameter λ for F18.

19V	19H	23V	37V	37H	92V	92V
0.720	0.720	0.793	0.773	0.773	0.976	0.976

In previous versions (Version 6 and Version 7), non-linearity was addressed via the so-called target factor adjustments. With the more direct nonlinearity adjustments described above, these adjustments are no longer needed. These are made possible by using GMI as a calibration reference. Version 6 and 7 calibration began with the first SSM/I (F08) and carried the calibration forward to more recent satellites. Version 8 takes the opposite approach. The calibration originates with the recent GPM Microwave Imager (GMI) instrument on the Global Precipitation Mission (GPM) satellite, and then proceeds backwards to earlier instruments, including SSMIS F18. The reason for this change is that the calibration of the GMI instrument is better understood than any previous instrument. This is in part because in addition to cold space and warm target calibration points, GMI includes an on-board noise source that injects ~100K of noise into the radiometer system, allowing for 2 additional calibration points, cold space + 100K, and the warm target + 100K. These additional points allow the non-linearity of the radiometer to be precisely measured for the first time. This, in turn, allows us to more precisely tie the absolute calibration of the GMI instrument to our radiative transfer model over a wide range of scene brightness temperatures, including both ocean (intermediate TB) and land (high TB). The GMI calibration procedure is described in detail in Wentz and Draper [2016].

The precise calibration of the GMI instrument allows us to develop a detailed model of the seasonal and diurnal variation of the brightness temperature of the surface emission from high TA land sources, in particular from the Amazon rain forest, which we have found to be relatively stable from year to year. This in turn allows the use of the Amazon as a third calibration point to assess the absolute calibration and non-linearity of other satellites, including F18. Note that without the third point, it is impossible to determine whether observed intersatellite differences are due to absolute calibration offsets, or to differences in radiometer non-linearity. In version 8, the non-linearity is determined as part of the calibration procedure by comparing collocated observations from different satellites over both ocean target and the Amazon rain forest.

In Figure 2, we show that several V8 calibrated satellites agree over the Amazon rainforest to ~0.1K. Similar agreement is achieved with the same calibration over ocean targets.

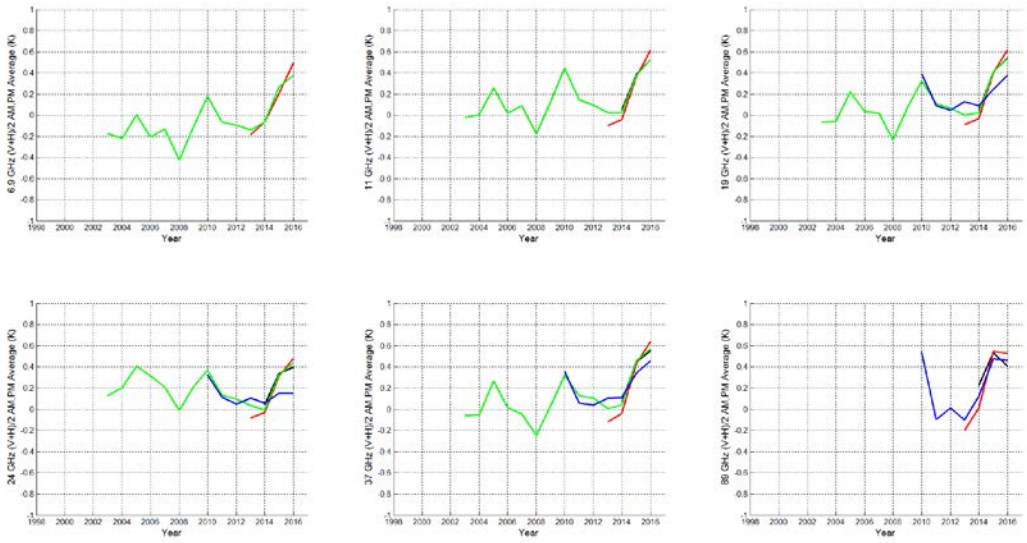

Figure 4. Comparison of AMSR-2 (red), GMI (black), WindSat (green), and F18 SSM/IS (blue) over the Amazon Rainforest. For all sensors, we show the difference between the brightness temperature (T_B) measurement minus the T_B model derived from NASA's precisely calibrated GMI sensor. The T_B value is the average of v-pol and h-pol. Also day and night observations have been averaged. All sensors show similar year-to-year variations, and this fact indicates the year-to-year variations seen in this figure are due to actual changes in the microwave emission from the Amazon rainforest rather than sensor calibration errors.

Absolute Calibration

As previously discussed, the antenna temperature is a measure of radiant power entering the feedhorn. It is the brightness temperature of the surrounding environment integrated over the gain pattern of the SSM/I parabolic reflector and feedhorn assembly. This integration can be well approximated by [*Wentz*, 1991]

$$T_{Ai} = q_i T_{Bi} + \chi_i q_i T_{Bj} + \eta_i T_{c,plk} \tag{23}$$

$$q_i = \frac{1-\eta_i}{1+\chi_i} \tag{24}$$

where the spillover η is the fraction of received power coming from cold space and the cross polarization coupling χ is fractional power coming from the orthogonal polarization. The subscript i denotes polarization: $i = v$ or h, and the subscript j denotes

the orthogonal polarization. When $i = v$, then $j = h$, and when $i = h$, then j = v. $T_{c,plk}$ is the Planck-adjusted value of cold space given in Section 3.4.3. The inverse of this relationship is called the antenna pattern correction (APC) and is given by

$$T_{Bi} = \frac{q_j T_{Ai} - \chi_i q_i T_{Aj} + \left(\chi_i q_i \eta_j - q_j \eta_i\right) T_{c,plk}}{q_i q_j \left(1 - \chi_i \chi_j\right)} \qquad (25)$$

In the more abbreviated notation used by equation (1) and (2), we let the antenna function $\Gamma(\mathbf{T_B})$ denote the conversion of T_B to T_A for all 7 radiometer channels, and likewise $\Gamma^{-1}(\mathbf{T_A})$ is the APC function for all channels.

There is no 22 GHz h-pol T_A measurement for SSM/I or SSMIS, and hence (25) cannot be used to find the 22 GHz T_B. To avoid this problem, the input to the geophysical retrieval algorithm is T_A rather than T_B, and the calibration is also done in terms of T_A rather than T_B, as discussed in Section 3.4.1. This avoids having to convert the single-pol 22 GHz T_A into a T_B.

Absolute calibration of the SSM/I or SSMIS T_A measurements to the RTM as dictated by (11) can be obtained by varying η and χ so that the mission averaged T_A measurements agree with RTM. Since there are two unknowns (η and χ) for each channel, the estimation must be constrained in some way. We make the assumption that η and χ are the same for both polarizations:

$$\eta_v = \eta_h$$
$$\chi_v = \chi_h \qquad (26)$$

For the dual polarization channels, the constraint imposed by (26) results in two unknowns for each polarization pair. The parameters η and χ are then varied to satisfy equation (11) for both polarizations.

At 22 GHz for which there is only the v-pol measurement, we need to employ an additional constraint to find both η and χ. The vapor retrievals for the F13 SSM/I are compared to collocated and validated WindSat vapor retrievals. The validation of the WindSat vapor retrievals is based on comparisons with GPS values, and these comparisons show good, unbiased agreement over the full range of water vapor from 0 to 65 mm. The vapor retrievals are driven by the 22-GHz measurements, and the 0 to 65 mm range corresponds to a range in the 22V T_A of about 75 K. This provides enough dynamic range to estimate both the offset and the slope of the SSM/I minus WindSat vapor difference. The parameters η and χ are found so as to make the SSM/I vapor retrievals agree with Windsat while satisfying equation (11). These two constraints then provide the means for finding both η and χ at 22 GHz. The value found for χ is 0.01560 as compared to the pre-launch value of 0.00983. This is a small change, equivalent to about 0.3 K in T_A. Rather than trying to do this type of analysis for each SSM/I, we simply use χ_{22v}=0.01560 for all SSM/Is and SSMIS. Having fixed χ_{22v}, then η_{22v} becomes the single parameter used to satisfy equation (11) for the other SSM/Is.

Assumption (26) that the spillover and polarization coupling is the same for both polarizations is supported by both pre-launch antenna pattern measurements and on-orbit SSM/I observations of heavily forested areas. *Hollinger et al.* [1987] report the same F08 SSM/I pre-launch spillover values for v-pol and h-pol. The reported polarization difference in χ ranged from 0.0006 to 0.005 (equivalent to about 0.05-0.25 K in T_A). Pre-launch antenna measurements of the other SSM/Is also indicate little polarization difference for η and χ [*Colton and Poe*, 1999].

The other evidence that supports (26) is the SSM/I observations of heavily forested areas where the v-pol and h-pol T_B are nearly the same. Setting $T_{Bv} = T_{Bh}$ in (23) gives

$$T_{Ai} = (1-\eta_i)T_B + \eta_i T_{c,plk} \qquad (27)$$

Analysis of the SSMIS T_A observations of these heavily forested areas shows little if any polarization difference. Hence according to (27), this implies $\eta_v = \eta_h$.

Table 4 give the spillover and polarization coupling for the SSMIS F18.. These values are from the final step in the calibration process that minimizes both $\mathbf{\delta E_p}(i, j)$ and $T_A - T_{A,rtm}$, as discussed in Section 3.4.2.

It should be noted that an error in η and an error in the hot target temperature T_h have nearly the same effect on the calculation of T_B. They both introduce a multiplicative bias in T_B. The 1 K reduction of the hot target temperature as given by the thermistors (see Section 4) results in our derived spillover values shown in Table 3 and Figure 2 being 0.004 higher. As Figure 2 shows, this increase in η results in slightly better agreement with the pre-launch values when considering all SSM/Is and all frequencies. We have observed the same phenomenon with AMSR-E, WindSat, and SSM/IS: decreasing the thermistor T_h by 1 K results in spillover values that better agree with pre-launch measurements. Whether this is real (i.e, the effective temperature of the hot target is indeed a little less than the thermistor value) is difficult to say for sure. In any event, for nearly all applications it does not matter whether you assign this small error to η or T_h.

Table 5. Spillover (η) and Polarization Coupling (χ) F18 SSMIS

	19V	19Hz	22V	37V	37H	92V	92H
η	0.03265	0.03268	0.01940	0.0170	0.016950	0.03264	0.03446
χ	0.01710	0.01710	0.015084	0.22618	0.02618	0.00930	0.00930

Along-Scan Correction

One of the first SSM/I calibration problems that was detected was an along-scan error [*Wentz*, 1991]. Towards the end of the Earth scan, the cold target mirror begins to intrude into the field of view of the feedhorn. As a result, the T_A measurements exhibit a systematic roll-off of about 1 K at the end of the scan. Our model for the along-scan error is to assume the radiation entering the feedhorn is a combination of Earth radiation $T_{A,earth}$ reflected off the parabolic antenna and cold space radiation $T_{c,plk}$ reflected off the cold target mirror:

$$T_{A0} = \left[1-\mu(\omega)\right]T_{A,earth} + \mu(\omega)T_{c,plk} \tag{28}$$

where $\mu(\omega)$ is a function of the along-scan position ω. Since $T_{A,earth}$ is the desired quantity, the required adjustment according to (12) and (28) is

$$\Delta T_{A,\omega} = \frac{-\mu(\omega)}{1-\mu(\omega)}\left(T_{A0} - T_{c,plk}\right) \tag{29}$$

Of the five relative T_A adjustments, the derivation of along-scan correction $\Delta T_{A,\omega}$ is probably the most straightforward and provides a good example of how inter-satellite T_A differences are used for the derivation. In this case we use the inter-satellite T_A differences $\delta T_A(i, j)$ defined by (14). $\mu(\omega)$ for F18 was determined via comparison with GMI. $\delta T_A(i, j)$ represent millions of collocated sensor-*i* minus sensor-*j* T_A differences. As discussed in Section 1.8.2, when computing $\delta T_A(i, j)$ all adjustments are applied other than the $\Delta T_{A,\omega}$ currently under consideration. Thus the assumption can be made that $\delta T_A(i, j)$ equals $\Delta T_{A,\omega}$. This assumption becomes more rigorous as the calibration procedure iterates and the various adjustments converged. Assuming $\delta T_A(i, j) = \Delta T_{A,\omega}$ and inverting (29) to yield $\mu(\omega)$ gives

$$\mu(\omega) = \frac{\delta T_A(i, j)}{\delta T_A(i, j) - \left(T_{A0} - T_{c,plk}\right)} \tag{30}$$

There are 64 scan positions for the 19-37 GHz channels and 128 positions for 85 GHz. Averages of $\mu(\omega)$ are found for each scan position thereby creating $\mu(\omega)$ tables. Figure 3 shows the $\mu(\omega)$ tables for SSMIS for all channels..

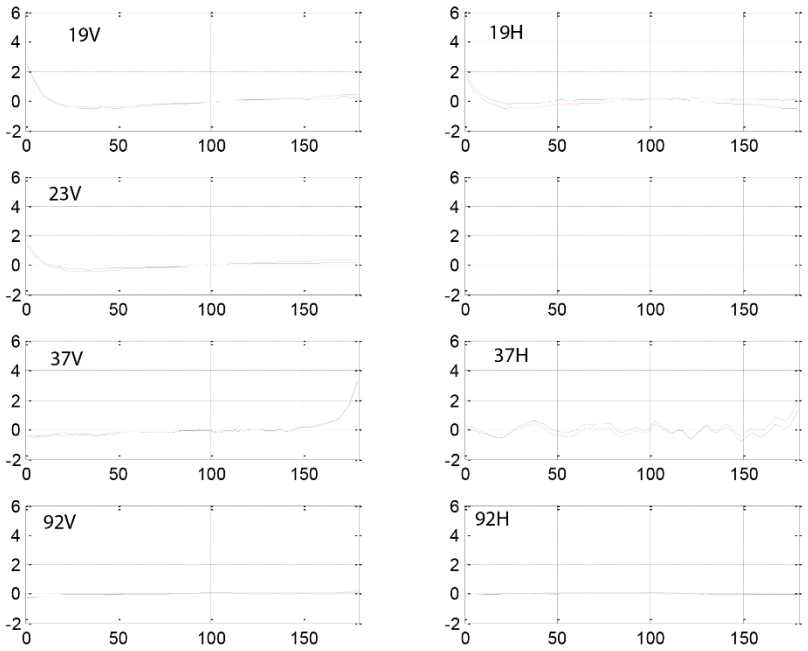

Figure 5. The along-scan correction that is applied to the SSMIS F18 T_A. To show these results in terms of a value indicative of the T_A adjustment, $\mu(\omega)$ has been multiplied by 200 K. The adjustment has the effect of increasing T_A at the ends of the scan to compensate for the intrusion of the cold mirror into the field of view. The 2 colors correspond ascending and descending nodes.

Adjustments to the Hot Target Temperature

As discussed in Section 3.4.3, the specification of the hot target temperature T_h is problematic. One must infer T_h from thermistor readings attached to the hot target. However, there will be some error in using these readings to estimate the effective emission temperature of the hot target. For example, the SSM/I has only 3 thermistors, and thermal gradients, both horizontal and vertical, over the extent of the hot target will introduce error. Such problems have been reported for both WindSat and the F16 SSM/IS [*Twarog et al*., 2006; *Sun and Weng*, 2008]. Herein, we find a similar, but smaller, problem for the F18 SSMIS.

The hot target temperature adjustment is found in a way analogous to that described in Section 3.4.5 for the along-scan correction. The change to T_A due to an error ΔT_h in specifying the hot target temperature is given by

$$\Delta T_{A,ht} = \frac{T_A - T_c}{T_h - T_c} \Delta T_h \qquad (31)$$

This is equivalent to adding ΔT_h to T_h in equation (19). Following the procedure described in Section 3.4.5, the assumption is made that $\delta T_A(i, j) = \Delta T_{A,ht}$ and (31) is inverted to yield ΔT_h.

$$\Delta T_h = \frac{T_h - T_c}{T_A - T_c} \delta T_A(i, j) \qquad (32)$$

To obtain a more robust estimate for ΔT_h, the assumption is made that ΔT_h is polarization independent (i.e., same for v-pol and h-pol). There is good physical and empirical justification for this assumption. Assuming ΔT_h is independent of polarization allows the usage the following linear combination of v-pol and h-pol T_A differences:

$$\delta T_{Ax}(i, j) = \delta T_{Av}(i, j) - \kappa \delta T_{Ah}(i, j) \qquad (33)$$

where the weighting coefficient $\kappa = 0.53$. This linear combination is selected because it is very insensitive to variations in the atmosphere moisture (i.e., V and L). Over the oceans, changes in atmospheric absorption due to either V or L affect h-pol about twice as much as v-pol, and hence $\delta T_{Ax}(i, j)$ is largely insensitive to these changes. The largest source of error in computing $\delta T_A(i, j)$ is the specification of V and L for $\mathbf{T}_{\mathbf{A,rtm}}(j)$, and using (33) greatly reduces this error. Combining (32) and (33) gives

$$\Delta T_h = \frac{(T_h - T_c)\delta T_{Ax}(i, j)}{T_{Av} - T_c - \kappa(T_{Ah} - T_c)} \qquad (34)$$

Equation (34) cannot be used for the 22 GHz channel because there is only a v-pol measurement. For this case, we use the 19 GHz ΔT_h to specify the 22 GHz value.

Analyses of hot target errors for WindSat [*Twarog et al*., 2006] and SSM/IS [*Sun and Weng*, 2008] indicate that at certain points in the orbit the sun shining on the hot target produces thermal gradients that are not captured by the thermistors. These events are typically characterized as 'solar intrusions' where the solar radiation either directly or via a reflection impinges onto the hot target. For these events the effective temperature of the hot target is not adequately represented by $T_{h,therm}$. The geometry of the solar intrusions can be complex with both direct and reflected intrusions causing problems. For the SSM/Is, rather than trying to explicitly model the geometry of the intrusions, we simply assume ΔT_h is a function of the sun's azimuth angle α and polar angle β as measured in the spacecraft coordinate system for which the z-axis points up away from nadir and the x-axis is the spacecraft velocity vector. We denote this function by $\Delta T_h(\alpha,$

β). Equation (34) is then used to make tables of $\Delta T_h(\alpha, \beta)$. The derivation of $\Delta T_h(\alpha, \beta)$ requires a pair of collocated imaging radiometers, in this case GMI and SSMIS F18.

In addition to $\Delta T_h(\alpha, \beta)$, there is a second adjustment that is made to the hot target temperature. This adjustment, which is applied to all SSM/Is, is based on the difference between the evening (pm) and morning (am) T_A measurements, and is denoted by $\Delta T_h(\psi, t)$, where ψ is the spacecraft angular position in orbit and t is time. The angle ψ equals 0 when the spacecraft is at its southern-most position in the orbit. This adjustment is modeled by a small but very systematic error we see between the pm and am measurements that we do not believe is due to real diurnal effects. The $\Delta T_h(\psi, t)$ adjustment is quite small, typically being ±0.2 K, and never exceeds ±0.5 K except at the very end of the missions for F10 and F15. The adjustment takes the form

$$\Delta T_h(\psi, t) = \left[G_0 + G_1(t) + G_{85}(t_{asc})\right]\sin\psi \qquad (35)$$

where G_0 is a constant that just depends on channel number and $G_1(t)$ is a slowly varying function of time t that is independent of channel number. The last term $G_{85}(t_{asc})$ is a special adjustment only applied to the 85 GHz channels. The derivation of these three terms and an explanation of how they are separated from the natural diurnal variation of $\mathbf{E_p}$ is given in Section 3.4.12.

The two hot target adjustments are then added together to obtain the total correction:

$$\Delta T_h = \Delta T_h(\alpha, \beta) + \Delta T_h(\psi, t) \qquad (36)$$

Figure 4 shows the Adjustments made to the hot load temperature for F18.

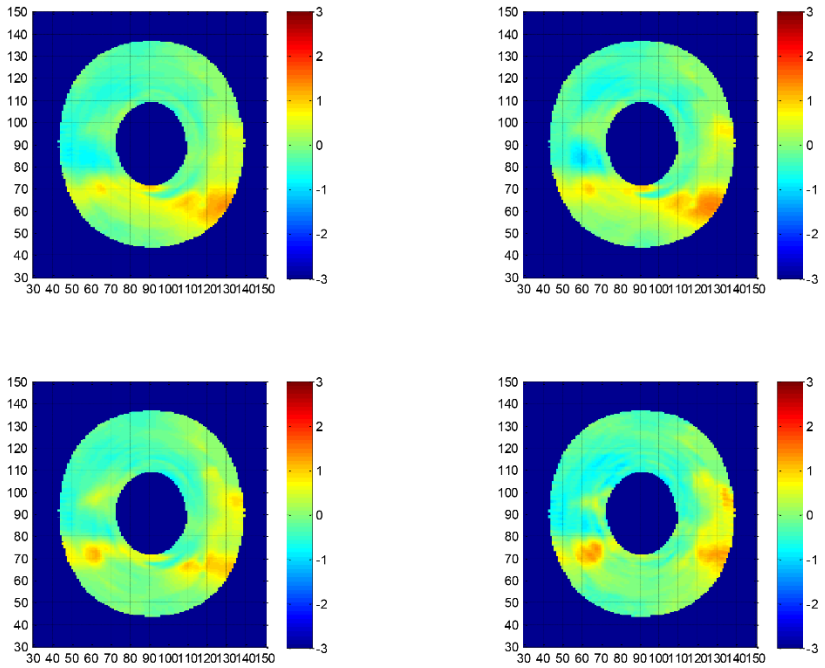

Figure 6. Adjustment to the hot target temperature ΔTh(α, β) to account for solar heating of the hot target. The four panels show the adjustments made to the 19GHz, 23 GHz, 37 GHZ, and 92 GHZ channels.

3.4.5 Look-Up Table Description

The following described the look-up tables used by the algorithm.

geo_coefs_f18.txt This is a text file containing coefficients used by the geolocation algorithm. The data is the first line are not used. The second line contains the cone angle each channel (19-37 GHz). The third line contains the starting azimuth angle for each channel. The next 6 lines contain the cold mirror vector in the spacecraft frame of reference for each channel. The cone angle and starting azimuth angle were derived using a combination of studies of the locations of coastlines, and by comparing measured and simulated brightess temperatures over the open ocean.

make_processing_weights_f_18.dat This file contains the resampling weights used by the resampling routine (resample_ta.f). The file is a flat binary file containing an array (1:90,-18:18,-14:14,3) of 4-byte reals. These coefficients were derived using the Backus-Gilbert method, which optimizes the noise performance for the resampled footprints.

xscan_table_f18.dat This file contains cross-scan corrections for each channel, cell, resampled footprint size, and polarization). The file is a flat binary file containing and array (4,90,4,2) of 4-byte reals. These were derived by the evaluation of brightness temperature errors as a function of scan position.

fd_tb_range_f18.lis This text file contains upper and lower bounds for brightness temperatures for each channel and polarization. These were derived by evaluating the range of algorithm output for tightly quality-controlled situations.

calibration_tables_f18.dat. This file contains 4 tables relating to calibration adjustments

1. dteff_alp_beta(0:359,0:359,8) array of 4 byte reals. This is an adjustment based on the alpha and beta angles for sun intrusion.
2. d_ant_temp(0:359,0:359) array of 4 byte reals. This is a temperature adjustment for the physical temperature of the dish as a function of sun alpha/betq
3. dish_ems(8,4) array of 4 byte reals. Adjustments to the dish emissivity for each chanel and footprint size
4. dta_zang (0:99,8) array of 4 byte reals. Adjustments to TA as a cunction of orbital position for each channel.

   These 4 tables are constructed by comparing m easured antenna temperatures with simulated antenna temperatures derived using geophysical measurements from other satellites, most importantly GMI.

apc_coefs_f18.txt Text file containing antenna pattern correction coefficients for each channel. These are derived from a combination of analysis of measured antenna patterns from pre-launch calibration, and the comparison of measured and simulated brightness temperatures.

3.4.6 Parameterization

Not Applicable

3.4.7 Algorithm Output

The algorithm output is RSS L1B brightness temperature data. One file is written for each SSM/I orbit. This data is then converted to netcdf4 using a IDL 8.2 routine. An example netcdf file name is:

RSS_SSMIS_FCDR_V08R00_F18_D20180101_S0100_E0252_R42312.nc

Where:

V08R00 corresponds to the version number

F18 is the satellite

20180101 is the year, month, and day of the start time

S0100 is the stat time in hhmm format

E0252 is the end time in hhmm format

R42312 refers to the obit number.

These files are then assembled into monthly tar files for transmission to NCEI.

An example monthly file name is:

RSS_SSMI_FCDR_V08R00_F18_D201603.tar

Where:

V08R00 corresponds to the version number

F18 is the satellite

D201603 refers to the year and month of the data.

4. Test Datasets and Outputs

4.1 Test Input Datasets

No formal test input datasets have been developed.

4.2 Test Output Analysis

4.2.1 Reproducibility

See comments in section 5.5 below.

4.2.2 Precision and Accuracy

See comments in Section 5.5 below.

4.2.3 Error Budget

The error in each brightness temperature measurement can be thought of coming from two sources. The first is radiometric noise from the sensor. This is controlled by the NEDT of the sensor, as modified by the noise reduction in the resampling algorithm. This part of the noise is fairly well understood. The second part of the error comes from systematic noise in the algorithm. This part of the error is very difficult to evaluate because no error-free comparison datasets exist. Comparison studies with other similar sensors (see section 5.5 below) suggest that the systematic error is on the order of a few 10^{th}'s of a degree K, which is comparable to the radiometric noise.

5. Practical Considerations

5.1 Numerical Computation Considerations

The algorithm is implemented using simple linear programming in FORTRAN (to do the calibration) and IDL (to write the netcdf files). No complex computation strategies were used. Since each orbital calculation is independent of any other, the computation can be performed in parallel by launching multiple instances.

5.2 Programming and Procedural Considerations

Not Applicable

5.3 Quality Assessment and Diagnostics

The use of quality flags variables in each netCDF file allows for detailed footprint-level identification of radiance anomalies.

5.4 Exception Handling

Algorithm input and intermediate results are checked to ensure that they are within reasonable bounds as the calculation proceeds. Out of bounds values are flagged, and the flags are propagated to the final NetCDF files.

5.5 Algorithm Validation

The primary validation of the V7 and V8 TA and TB datasets is through their resulting geophysical retrievals. For example, one of the most critical requirements for an CDR dataset is that it be free of spurious long-term trends. Validation of this requirement can be obtained by analyses of the resulting geophysical retrievals. Comparison of the wind speeds retrieved from the V6 TB with buoys and scatterometers indicates a trend error of 0.05 m/s/decade at the 95% confidence level over the 1987 to 2006 time period [Wentz et al., 2007]. The standard error on the water vapor trend (1987-2006) is 0.2% per decade [Wentz and Schabel, 2000]. With respect to precipitation, when diurnal effects are removed, the agreement among different SSM/I is 3% [Hilburn and Wentz, 2008b]. Note that some of this 3% difference is probably due to residual geophysical effects such as 'beamfilling' rather than TB intercalibration error. Still, 3% is the best inter-sensor precipitation agreement yet achieved from any SSM/I TB dataset.

In addition, the final brightness temperatures are compared with results from GMI.using simulated Tb values derived from GMI observations. Figure 5 shows the difference between T_B (F18) minus Tb,Sim(GMI) as a function of orbit number and and orbital position. For the 19GHZ, 23 GHz, and 37GHz channels, the agreement is very good. For the 92 GHz channels, the agreement is somewhat worse, likely because of errors in cloud retrieval. For GMI, the high frequency channel is not used for the RSS cloud retrievals.

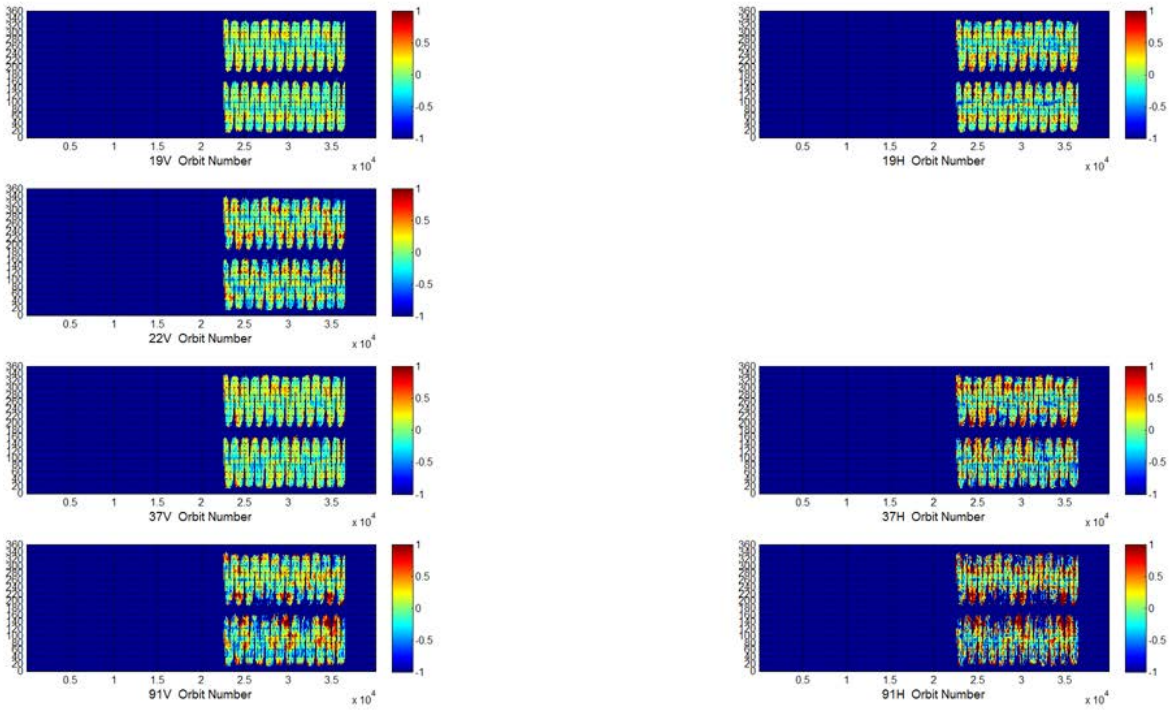

Figure 7 Comparison of Final Tb values with GMI results, using similar SSMIS TB's derived from GMI physical retrievals.

5.6 Processing Environment and Resources

The code was developed on a windows workstation running windows 10. FORTRAN was compiled using the Intel FORTRAN compiler, and IDL V8.0 was used to write the netcdf files. Large amounts of memory or storage are not required, beyond the ability to store the input L1A files, and the outputted L1B files.

6. Assumptions and Limitations

The parameters in the various look-up tables were developed using the part of sun-angle space (alpha and beta) that the satellite has already sampled. We assume that future sun angle values will continue to fall in this space. Changes in orbital parameters that result in new areas of sun angle will result in sun angles flagged as out of bounds, and the calibration procedure needs to be repeated.

6.1 Algorithm Performance

Describe all assumptions that have been made concerning algorithm performance. To the extent possible, the potential for degraded performance should be explored, along with mitigating strategies.

<Enter Text Here>

6.2 Sensor Performance

It is implicit in our analysis that the sensor will continue to perform as it has been performing. Any sensor anomalies can result in errors in the output brightness temperatures, at least until the anomalies are studied and corrected for.

7. Future Enhancements

7.1 Enhancement 1

Extend the V8 calibration standard to other satellites in the SSMIS and SSM/I series. This will proceed backward in time, starting with F17.

8. References

Christy, J. R., R. W. Spencer, et al. (2000), MSU Tropospheric Temperatures: Dataset Construction and Radiosonde Comparisons, *Journal of Atmospheric and Oceanic Technology, 17*(9): 1153-1170.

Colton, M. C. and G. A. Poe (1999), Intersensor Calibration of DMSP SSM/I's: F-8 to F-14, 1987-1997, *IEEE Trans. Geoscience and Remote Sensing, 37*, 418-439.

Hilburn, K. A. and F. J. Wentz (2008), Mitigating the Impact of RADCAL Beacon Contamination on F15 SSM/I Ocean Retrievals. *Geophysical Research Letters, 35.* L18806, doi:10.1029/2008GL034914.

Hilburn, K. A. (2009), Including Temperature Effects in the F15 RADCAL Correction. *RSS Technical Report 051209*, , Remote Sensing Systems, Santa Rosa, CA, http://www.remss.com/papers/RSS_TR051209_RADCAL.pdf

Hollinger,J., R. Lo, G. Poe, R. Savage, and J. Pierce (1987), Special Sensor Mirowave/Imager User's Guide, *Naval Research Laboratory Report*, Washington DC.

Mears, C. A., M. C. Schabel, and F. J. Wentz (2003), A Reanalysis of the MSU Channel 2 Tropospheric Temperature Record. *Journal of Climate, 16*, 3650-3664.

Meissner, T. and F. Wentz (2002), *An updated analysis of the ocean surface wind direction signal in passive microwave brightness temperatures IEEE Trans. Geoscience and Remote Sensing, 40*(6), 1230.

Meissner, T. and F. Wentz (2003), *A radiative transfer model function for 85.5 GHz SSM/I ocean brightness temperatures*, *Radio Science, 38*(4), 8066.

Meissner, T. and F. Wentz (2004), *The complex dielectric constant of pure and sea water from microwave satellite observations*, *IEEE Trans. Geoscience and Remote Sensing*, *42*(9), 1836.

Meissner. T., and F. Wentz (2012), *The emissivity of the ocean surface between 6 - 90 GHz over a large range of wind speeds and Earth incidence angles*, *IEEE Trans. Geoscience and Remote Sensing, 50*(8), 3004.

Smith, D. K., C. A. Mears, and F. J. Wentz (2002), Detection and characterization of diurnal winds using QuikScat data, *2002 International Geoscience and Remote Sensing Symposium*, IGARSS, IEEE, Toronto, Canada, 735-737.

Sun, N. and Fuzhong Weng (2008), Evaluation of Special Sensor Microwave Imager/Sounder (SSMIS) Environmental Data Records, *IEEE Trans. Geoscience and Remote Sensing, 46*(4) 1006-1016

Twarog, E. M., W. E. Purdy, P. W. Gaiser, K. H. Cheung, and B. E. Kelm (2006), **WindSat On-Orbit Warm Load Calibration*, IEEE Trans. Geoscience and Remote Sensing 44*(3) 516-529.**

Wentz, F. J. (1983), A model function for ocean microwave brightness temperatures, *J. Geophy. Res. 88,* 1892-1908.

Wentz, F. J. (1988), User's Manual SSM/I Antenna Temperature Tapes. *RSS Technical Report 032588*, Remote Sensing Systems, Santa Rosa, CA.

Wentz, F. J., (1991), Revision 1 User's Manual SSM/I Antenna Temperature Tapes. *RSS Technical Report 120191*, Remote Sensing Systems, Santa Rosa, CA. http://www.remss.com/papers/ssmi/TA/SSMI_TA_manual_rev_1_part_1.pdf, http://www.remss.com/papers/ssmi/TA/SSMI_TA_manual_rev_1_part_2.pdf

Wentz, F. J., (1993), Revision 2 User's Manual SSM/I Antenna Temperature Tapes. *RSS Technical Report 120193*, Remote Sensing Systems, Santa Rosa, CA. http://www.remss.com/papers/ssmi/TA/SSMI_TA_manual_rev_2.pdf

Wentz, F. J., (1997), A Well Calibrated Ocean Algorithm for Special Sensor Microwave/Imager*, J. of Geophysical Research, 102*, 8703-8718.

Wentz, F. and T. Meissner (2000), *AMSR Ocean Algorithm (Version 2) Algorithm Theoretical Basis Document (ATBD)*, *RSS Technical Report 121599A-1*, Remote Sensing Systems, Santa Rosa, CA, http://www.remss.com/papers/amsr/AMSR_Ocean_Algorithm_Version_2.pdf.

Wentz, F. J. (2010), The Version-6 Calibration of SSM/I, *RSS Technical Report 102210*, Remote Sensing Systems, Santa Rosa, CA. http://www.remss.com/papers/tech_reports/Wentz_SSMI_Version6_Calibration.pdf

Wentz, F. J., & Draper, D. (2016). On-Orbit Absolute Calibration of the Global Precipitation Measurement Microwave Imager. *Journal of Atmospheric and Oceanic Technology, 33*, 1393-1412. *https://doi.org/10.1175/JTECH-D-15-0212.1*

Wentz, F.J., and T. Meissner, 2016, Atmospheric Absorption Model for Dry Air and Water Vapor at Microwave Frequencies below 100 GHz Derived from Spaceborne Radiometer Observations, *Radio Science*, 51, doi:10.1002/2015RS005858.

Appendix A. Acronyms and Abbreviations

Acronym or Abbreviation	Definition
AMSU	Advanced Microwave Sounding Unit
CATBD	Climate Algorithm Theoretical Basis Document
CDR	Climate Data Record
DMSP	Defense Meteorological Satellite Program
GMI	GPM Microwave Imager
GPM	Global Precipitation Mission
EUMETSAT	European Organisation for the Exploitation of Meteorological Satellites
FCDR	Fundamental Climate Data Record
GMAO	Global Modeling and Assimilation Office
GPCP	Global Precipitation Climatology Project
MEaSUREs	Making Earth Science Data Records for Use in Research Environments
MSU	Microwave Sounding Unit
NASA	National Aeronautics and Space Administration
NCDC	National Climatic Data Center
netCDF-4	network Common Data Form, Version 4.x
NOAA	National Oceanic and Atmospheric Administration
NSIDC	National Snow and Ice Data Center
RADCAL	Radar Calibration
REASoN	Research, Education and Applications Solution Network
RSS	Remote Sensing Systems
SBIR	Small Business Innovation Research
SSM/I	Special Sensor Microwave/Imager
T_A	Antenna temperature
T_B	Brightness temperature